6 Flexural Vibration of Plates

Flat plate structures, such as the floors of aircraft, buildings and ships, bridge decks and enclosures surrounding machinery, are subject to dynamic loads normal to their plane. This results in flexural vibration. Such structures can be analysed by dividing the plate up into an assemblage of two-dimensional finite elements called plate bending elements. These elements may be either triangular, rectangular or quadrilateral in shape.

The energy expressions for a thin plate bending element are, from Section 2.6,

$$T_e = \frac{1}{2}\int_A \rho h \dot{w}^2 \, \mathrm{d}A \tag{6.1}$$

$$U_e = \frac{1}{2}\int_A \frac{h^3}{12} \{\boldsymbol{\chi}\}^{\mathrm{T}} [\mathbf{D}] \{\boldsymbol{\chi}\} \, \mathrm{d}A \tag{6.2}$$

with

$$\{\boldsymbol{\chi}\} = \begin{bmatrix} \partial^2 w/\partial x^2 \\ \partial^2 w/\partial y^2 \\ 2\partial^2 w/\partial x \partial y \end{bmatrix} \tag{6.3}$$

where $[\mathbf{D}]$ is defined by (2.45), (2.49) or (2.51) depending upon whether the material is anisotropic, orthotropic or isotropic. Also

$$\delta W_e = \int_A p_z \delta w \, \mathrm{d}A \tag{6.4}$$

The highest derivative appearing in these expressions is the second. Hence, for convergence, it will be necessary to ensure that w and its first derivatives $\partial w/\partial x$ and $\partial w/\partial y$ are continuous between elements. These three quantities are, therefore, taken as degrees of freedom at each node. Also, complete polynomials of at least degree two should be used (see Section 3.2). The assumed form of the displacement function, whatever the element shape, is

$$w = \alpha_1 + \alpha_2 x + \alpha_3 y + \alpha_4 x^2 + \alpha_5 xy + \alpha_6 y^2 + \text{higher degree terms} \tag{6.5}$$

https://doi.org/10.1017/CBO9780511761195.008 Published online by Cambridge University Press

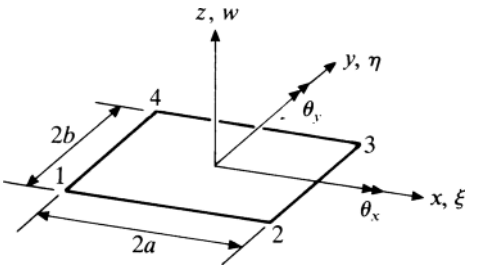

Figure 6.1. Geometry of a rectangular element. $\xi = x/a$, $\eta = y/b$.

6.1 Thin Rectangular Element (non-conforming)

Figure 6.1 shows a rectangular element with four node points, one at each corner. There are three degrees of freedom at each node, namely, the component of displacement normal to the plane of the plate, w, and the two rotations $\theta_x = \partial w/\partial y$ and $\theta_y = -\partial w/\partial x$. In terms of the (ξ, η) coordinates, these become

$$\theta_x = \frac{1}{b}\frac{\partial w}{\partial \eta}, \qquad \theta_y = -\frac{1}{a}\frac{\partial w}{\partial \xi} \tag{6.6}$$

Since the element has twelve degrees of freedom, the displacement function can be represented by a polynomial having twelve terms, that is

$$\begin{aligned} w = {} & \alpha_1 + \alpha_2\xi + \alpha_3\eta + \alpha_4\xi^2 + \alpha_5\xi\eta + \alpha_6\eta^2 \\ & + \alpha_7\xi^3 + \alpha_8\xi^2\eta + \alpha_9\xi\eta^2 + \alpha_{10}\eta^3 + \alpha_{11}\xi^3\eta + \alpha_{12}\xi\eta^3 \end{aligned} \tag{6.7}$$

Note that this function is a complete cubic to which has been added two quartic terms $\xi^3\eta$ and $\xi\eta^3$ which are symmetrically placed in Pascal's triangle (Figure 4.1). This will ensure that the element is geometrically invariant (see Chapter 4).

The expression (6.7) can be written in the following matrix form

$$\begin{aligned} w &= \lfloor 1 \quad \xi \quad \eta \quad \xi^2 \quad \xi\eta \quad \eta^2 \quad \xi^3 \quad \xi^2\eta \quad \xi\eta^2 \quad \eta^3 \quad \xi^3 n \quad \xi\eta^3 \rfloor \{\boldsymbol{\alpha}\} \\ &= \lfloor \mathbf{P}(\xi, \eta) \rfloor \{\boldsymbol{\alpha}\} \end{aligned} \tag{6.8}$$

where

$$\{\boldsymbol{\alpha}\}^{\mathrm{T}} = \lfloor \alpha_1 \quad \alpha_2 \quad \cdots \quad \alpha_{12} \rfloor \tag{6.9}$$

Differentiating (6.8) gives

$$\frac{\partial w}{\partial \xi} = \lfloor 0 \quad 1 \quad 0 \quad 2\xi \quad \eta \quad 0 \quad 3\xi^2 \quad 2\xi\eta \quad \eta^2 \quad 0 \quad 3\xi^2\eta \quad \eta^3 \rfloor \{\boldsymbol{\alpha}\} \tag{6.10}$$

and

$$\frac{\partial w}{\partial \eta} = \lfloor 0 \quad 0 \quad 1 \quad 0 \quad \xi \quad 2\eta \quad 0 \quad \xi^2 \quad 2\xi\eta \quad 3\eta^2 \quad \xi^3 \quad 3\xi\eta^2 \rfloor \{\boldsymbol{\alpha}\} \tag{6.11}$$

Evaluating (6.8), (6.10) and (6.11) at $\xi = \mp 1$, $\eta = \mp 1$ gives

$$\{\bar{\mathbf{w}}\}_e = [\mathbf{A}]_e \{\boldsymbol{\alpha}\} \tag{6.12}$$

where

$$\{\bar{\mathbf{w}}\}_e^{\mathrm{T}} = \lfloor w_1 \quad b\theta_{x1} \quad a\theta_{y1} \quad \cdots \quad w_4 \quad b\theta_{x4} \quad a\theta_{y4} \rfloor \tag{6.13}$$

https://doi.org/10.1017/CBO9780511761195.008 Published online by Cambridge University Press

and

$$[\mathbf{A}]_e = \begin{bmatrix} 1 & -1 & -1 & 1 & 1 & 1 & -1 & -1 & -1 & -1 & 1 & 1 \\ 0 & 0 & 1 & 0 & -1 & -2 & 0 & 1 & 2 & 3 & -1 & -3 \\ 0 & -1 & 0 & 2 & 1 & 0 & -3 & -2 & -1 & 0 & 3 & 1 \\ 1 & 1 & -1 & 1 & -1 & 1 & 1 & -1 & 1 & -1 & -1 & -1 \\ 0 & 0 & 1 & 0 & 1 & -2 & 0 & 1 & -2 & 3 & 1 & 3 \\ 0 & -1 & 0 & -2 & 1 & 0 & -3 & 2 & -1 & 0 & 3 & 1 \\ 1 & 1 & 1 & 1 & 1 & 1 & 1 & 1 & 1 & 1 & 1 & 1 \\ 0 & 0 & 1 & 0 & 1 & 2 & 0 & 1 & 2 & 3 & 1 & 3 \\ 0 & -1 & 0 & -2 & -1 & 0 & -3 & -2 & -1 & 0 & -3 & -1 \\ 1 & -1 & 1 & 1 & -1 & 1 & -1 & 1 & -1 & 1 & -1 & -1 \\ 0 & 0 & 1 & 0 & -1 & 2 & 0 & 1 & -2 & 3 & -1 & -3 \\ 0 & -1 & 0 & 2 & -1 & 0 & -3 & 2 & -1 & 0 & -3 & -1 \end{bmatrix} \tag{6.14}$$

Solving (6.12) for $\{\boldsymbol{\alpha}\}$ gives

$$\{\boldsymbol{\alpha}\} = [\mathbf{A}]_e^{-1} \{\bar{\mathbf{w}}\}_e \tag{6.15}$$

where

$$[\mathbf{A}]_e^{-1} = \frac{1}{8} \begin{bmatrix} 2 & 1 & -1 & 2 & 1 & 1 & 2 & -1 & 1 & 2 & -1 & -1 \\ -3 & -1 & 1 & 3 & 1 & 1 & 3 & -1 & 1 & -3 & 1 & 1 \\ -3 & -1 & 1 & -3 & -1 & -1 & 3 & -1 & 1 & 3 & -1 & -1 \\ 0 & 0 & 1 & 0 & 0 & -1 & 0 & 0 & -1 & 0 & 0 & 1 \\ 4 & 1 & -1 & -4 & -1 & -1 & 4 & -1 & 1 & -4 & 1 & 1 \\ 0 & -1 & 0 & 0 & -1 & 0 & 0 & 1 & 0 & 0 & 1 & 0 \\ 1 & 0 & -1 & -1 & 0 & -1 & -1 & 0 & -1 & 1 & 0 & -1 \\ 0 & 0 & -1 & 0 & 0 & 1 & 0 & 0 & -1 & 0 & 0 & 1 \\ 0 & 1 & 0 & 0 & -1 & 0 & 0 & 1 & 0 & 0 & -1 & 0 \\ 1 & 1 & 0 & 1 & 1 & 0 & -1 & 1 & 0 & -1 & 1 & 0 \\ -1 & 0 & 1 & 1 & 0 & 1 & -1 & 0 & -1 & 1 & 0 & -1 \\ -1 & -1 & 0 & 1 & 1 & 0 & -1 & 1 & 0 & 1 & -1 & 0 \end{bmatrix} \tag{6.16}$$

Substituting (6.15) into (6.8) gives

$$\begin{aligned} w &= \lfloor \mathbf{N}_1(\xi, \eta) \quad \mathbf{N}_2(\xi, \eta) \quad \mathbf{N}_3(\xi, \eta) \quad \mathbf{N}_4(\xi, \eta) \rfloor \{\mathbf{w}\}_e \\ &= \lfloor \mathbf{N}(\xi, \eta) \rfloor \{\mathbf{w}\}_e \end{aligned} \tag{6.17}$$

where

$$\{\mathbf{w}\}_e^{\mathrm{T}} = \lfloor w_1 \quad \theta_{x1} \quad \theta_{y1} \quad \cdots \quad w_4 \quad \theta_{x4} \quad \theta_{y4} \rfloor \tag{6.18}$$

and

$$\mathbf{N}_j^{\mathrm{T}}(\xi, \eta) = \begin{bmatrix} \frac{1}{8}(1 + \xi_j \xi)(1 + \eta_j \eta)(2 + \xi_j \xi + \eta_j \eta - \xi^2 - \eta^2) \\ (b/8)(1 + \xi_j \xi)(\eta_j + \eta)(\eta^2 - 1) \\ -(a/8)(\xi_j + \xi)(\xi^2 - 1)(1 + \eta_j \eta) \end{bmatrix} \tag{6.19}$$

(ξ_j, η_j) are the coordinates of node j. This element is commonly referred to as the ACM element [6.1, 6.2].

https://doi.org/10.1017/CBO9780511761195.008 Published online by Cambridge University Press

Evaluating (6.19) on the side 2–3 (i.e., $\xi = +1$) gives

$$\mathbf{N}_1^{\mathrm{T}} = \begin{bmatrix} 0 \\ 0 \\ 0 \end{bmatrix}, \qquad \mathbf{N}_2^{\mathrm{T}} \begin{bmatrix} \frac{1}{4}(1-\eta)(2-\eta-\eta^2) \\ (b/4)(-1+\eta)(\eta^2-1) \\ 0 \end{bmatrix}$$
$$\mathbf{N}_3^{\mathrm{T}} = \begin{bmatrix} \frac{1}{4}(1+\eta)(2+\eta-\eta^2) \\ (b/4)(1+\eta)(\eta^2-1) \\ 0 \end{bmatrix}, \qquad \mathbf{N}_4^{\mathrm{T}} = \begin{bmatrix} 0 \\ 0 \\ 0 \end{bmatrix} \tag{6.20}$$

This indicates that the displacement, and hence the rotation θ_x, is uniquely determined by the values of w and θ_x at nodes 2 and 3. Therefore, if the element is attached to another rectangular element at nodes 2 and 3, then w and θ_x will be continuous along the common side. The rotation θ_y is given by

$$\begin{aligned} \theta_y &= -\frac{1}{a}\frac{\partial w}{\partial \xi} \\ &= -\frac{1}{a}\begin{bmatrix} \dfrac{\partial \mathbf{N}_1}{\partial \xi} & \cdots & \dfrac{\partial \mathbf{N}_4}{\partial \xi} \end{bmatrix} \{\mathbf{w}\}_e \end{aligned} \tag{6.21}$$

(see equations (6.6) and (6.17)). Substituting (6.19) into (6.21) and evaluating along $\xi = +1$ gives

$$\frac{\partial \mathbf{N}_j^{\mathrm{T}}}{\partial \xi} = \begin{bmatrix} \frac{1}{8}(1+\eta_j\eta)\left(-2+2\xi_j^2+\xi_j\eta_j\eta-\xi_j\eta^2\right) \\ (b/8)\xi_j(\eta_j+\eta)(\eta^2-1) \\ -(a/8)(2+2\xi_j)(1+\eta_j\eta) \end{bmatrix} \tag{6.22}$$

Evaluating (6.22) for $j = 1$ to 4 gives

$$\frac{\partial \mathbf{N}_1^{\mathrm{T}}}{\partial \xi} = \begin{bmatrix} \frac{1}{8}\eta(1-\eta^2) \\ -(b/8)(-1+\eta)(\eta^2-1) \\ 0 \end{bmatrix},$$
$$\frac{\partial \mathbf{N}_2^{\mathrm{T}}}{\partial \xi} = \begin{bmatrix} -\frac{1}{8}\eta(1-\eta^2) \\ (b/8)(-1+\eta)(\eta^2-1) \\ -(a/2)(1-\eta) \end{bmatrix}$$
$$\frac{\partial \mathbf{N}_3^{\mathrm{T}}}{\partial \xi} = \begin{bmatrix} \frac{1}{8}\eta(1-\eta^2) \\ (b/8)(1+\eta)(\eta^2-1) \\ -(a/2)(1+\eta) \end{bmatrix}, \tag{6.23}$$
$$\frac{\partial \mathbf{N}_4^{\mathrm{T}}}{\partial \xi} = \begin{bmatrix} -\frac{1}{8}\eta(1-\eta^2) \\ -(b/8)(1+\eta)(\eta^2-1) \\ 0 \end{bmatrix}$$

For θ_y to be continuous between elements it should be uniquely determined by its value at nodes 2 and 3. Expressions (6.21) and (6.23) indicate that in this case θ_y is determined by the values of w and θ_x at nodes 1, 2, 3 and 4 as well as θ_y at

https://doi.org/10.1017/CBO9780511761195.008 Published online by Cambridge University Press

nodes 2 and 3. The element is, therefore, a non-conforming one. In spite of this, the element is used and will, therefore, be considered further and the effect of this lack of continuity indicated.

Substituting (6.17) into (6.1) gives

$$T_e = \tfrac{1}{2}\{\dot{\mathbf{w}}\}_e^{\mathrm{T}}[\mathbf{m}]_e[\dot{\mathbf{w}}]_e \tag{6.24}$$

where

$$\begin{aligned}[\mathbf{m}]_e &= \int_{A_e} \rho h \lfloor \mathbf{N} \rfloor^{\mathrm{T}} \lfloor \mathbf{N} \rfloor \, \mathrm{d}A \\ &= \rho hab \int_{-1}^{+1}\int_{-1}^{+1} \lfloor \mathbf{N}(\xi,\eta) \rfloor^{\mathrm{T}} \lfloor \mathbf{N}(\xi,\eta) \rfloor \, \mathrm{d}\xi \, \mathrm{d}\eta \end{aligned} \tag{6.25}$$

is the element inertia matrix. Substituting the functions $\mathbf{N}_j(\xi,\eta)$ from (6.19) and integrating gives

$$[\mathbf{m}]_e = \frac{\rho hab}{6300}\begin{bmatrix} \mathbf{m}_{11} & \mathbf{m}_{12}^{\mathrm{T}} \\ \mathbf{m}_{21} & \mathbf{m}_{22} \end{bmatrix} \tag{6.26}$$

where

$$\mathbf{m}_{11} = \begin{bmatrix} 3454 & & & & & \\ 922b & 320b^2 & & & \text{Sym} & \\ -922a & -252ab & 320a^2 & & & \\ 1226 & 398b & -548a & 3454 & & \\ 398b & 160b^2 & -168ab & 922b & 320b^2 & \\ 548a & 168ab & -240a^2 & 922a & 252ab & 320a^2 \end{bmatrix} \tag{6.27}$$

$$\mathbf{m}_{21} = \begin{bmatrix} 394 & 232b & -232a & 1226 & 548b & 398a \\ -232b & -120b^2 & 112ab & -548b & -240b^2 & -168ab \\ 232a & 112ab & -120a^2 & 398a & 168ab & 160a^2 \\ 1226 & 548b & -398a & 394 & 232b & 232a \\ -548b & -240b^2 & 168ab & -232b & -120b^2 & -112ab \\ -398a & -168ab & 160a^2 & -232a & -112ab & -120a^2 \end{bmatrix} \tag{6.28}$$

and

$$\mathbf{m}_{22} = \begin{bmatrix} 3454 & & & & & \\ -922b & 320b^2 & & & \text{Sym} & \\ 922a & -252ab & 320a^2 & & & \\ 1226 & -398b & 548a & 3454 & & \\ -398b & 160b^2 & -168ab & -922b & 320b^2 & \\ -548a & 168ab & -240a^2 & -922a & 252ab & 320a^2 \end{bmatrix} \tag{6.29}$$

https://doi.org/10.1017/CBO9780511761195.008 Published online by Cambridge University Press

In deriving this result, it is simpler to use the expression (6.8) for w and substitute for $\{\boldsymbol{\alpha}\}$ after performing the integration. A typical integral is then of the form

$$\int_{-1}^{+1}\int_{-1}^{+1} \xi^m \eta^n \,\mathrm{d}\xi\,\mathrm{d}\eta = \begin{cases} 0 & m \text{ or } n \text{ odd} \\ \dfrac{4}{(m+1)(n+1)} & m \text{ and } n \text{ even} \end{cases} \tag{6.30}$$

Substituting (6.17) into (6.3) and (6.2) gives

$$U_e = \tfrac{1}{2}\{\mathbf{w}\}_e^{\mathrm{T}}[\mathbf{k}]_e\{\mathbf{w}\}_e \tag{6.31}$$

where

$$[\mathbf{k}]_e = \int_{A_e} \frac{h^3}{12}\,[\mathbf{B}]^{\mathrm{T}}\,[\mathbf{D}]\,[\mathbf{B}]\,\mathrm{d}A \tag{6.32}$$

is the element stiffness matrix, and

$$[\mathbf{B}] = \begin{bmatrix} \dfrac{\partial^2}{\partial x^2} \\ \dfrac{\partial^2}{\partial y^2} \\ 2\dfrac{\partial^2}{\partial x\,\partial y} \end{bmatrix} \lfloor \mathbf{N} \rfloor = \begin{bmatrix} \dfrac{1}{a^2} & \dfrac{\partial^2}{\partial \xi^2} \\ \dfrac{1}{b^2} & \dfrac{\partial^2}{\partial \eta^2} \\ \dfrac{2}{ab} & \dfrac{\partial^2}{\partial \xi\,\partial \eta} \end{bmatrix} \lfloor \mathbf{N}(\xi,\eta) \rfloor \tag{6.33}$$

Substituting the functions $\mathbf{N}_j(\xi,\eta)$ from (6.19) and integrating gives, for the isotropic case

$$[\mathbf{k}]_e = \frac{Eh^3}{48(1-\nu^2)ab} \begin{bmatrix} \mathbf{k}_{11} & & \text{Sym} & \\ \mathbf{k}_{21} & \mathbf{k}_{22} & & \\ \mathbf{k}_{31} & \mathbf{k}_{32} & \mathbf{k}_{33} & \\ \mathbf{k}_{41} & \mathbf{k}_{42} & \mathbf{k}_{43} & \mathbf{k}_{44} \end{bmatrix} \tag{6.34}$$

where

$$\mathbf{k}_{11} = \begin{bmatrix} \left\{4(\beta^2+\alpha^2) + \frac{2}{5}(7-2\nu)\right\} & & \text{Sym} \\ 2\left\{2\alpha^2 + \frac{1}{5}(1+4\nu)\right\} b & 4\left\{\frac{4}{3}\alpha^2 + \frac{4}{15}(1-\nu)\right\} b^2 & \\ 2\left\{-2\beta^2 - \frac{1}{5}(1-4\nu)\right\} a & -4\nu ab & 4\left\{\frac{4}{3}\beta^2 + \frac{1}{15}(1-\nu)\right\} a^2 \end{bmatrix} \tag{6.35}$$

$$\mathbf{k}_{21} = \begin{bmatrix} -\left\{2(2\beta^2-\alpha^2) + \frac{2}{5}(7-2\nu)\right\} & 2\left\{\alpha^2 - \frac{1}{5}(1+4\nu)\right\} b & 2\left\{2\beta^2 + \frac{1}{5}(1-\nu)\right\} a \\ 2\left\{\alpha^2 - \frac{1}{5}(1+4\nu)\right\} b & 4\left\{\frac{2}{3}\alpha^2 - \frac{4}{15}(1-\nu)\right\} b^2 & 0 \\ -2\left\{2\beta^2 + \frac{1}{5}(1-\nu)\right\} a & 0 & 4\left\{\frac{2}{3}\beta^2 - \frac{1}{15}(1-\nu)\right\} a^2 \end{bmatrix} \tag{6.36}$$

https://doi.org/10.1017/CBO9780511761195.008 Published online by Cambridge University Press

$$\mathbf{k}_{31} = \begin{bmatrix} -\left\{2(\beta^2+\alpha^2) - \frac{2}{5}(7-2\nu)\right\} & 2\left\{-\alpha^2 + \frac{1}{5}(1-\nu)\right\} b & 2\left\{\beta^2 - \frac{1}{5}(1-\nu)\right\} a \\ 2\left\{\alpha^2 - \frac{1}{5}(1-\nu)\right\} b & 4\left\{\frac{1}{3}\alpha^2 + \frac{1}{15}(1-\nu)\right\} b^2 & 0 \\ 2\left\{-\beta^2 + \frac{1}{5}(1-\nu)\right\} a & 0 & 4\left\{\frac{1}{3}\beta^2 + \frac{1}{15}(1-\nu)\right\} a^2 \end{bmatrix} \tag{6.37}$$

$$\mathbf{k}_{41} = \begin{bmatrix} \left\{2(\beta^2-2\alpha^2) - \frac{2}{5}(7-2\nu)\right\} & 2\left\{-2\alpha^2 - \frac{1}{5}(1-\nu)\right\} b & 2\left\{-\beta^2 + \frac{1}{5}(1+4\nu)\right\} a \\ 2\left\{2\alpha^2 + \frac{1}{5}(1-\nu)\right\} b & 4\left\{\frac{2}{3}\alpha^2 - \frac{1}{15}(1-\nu)\right\} b^2 & 0 \\ 2\left\{-\beta^2 + \frac{1}{5}(1+4\nu)\right\} a & 0 & 4\left\{\frac{2}{3}\beta^2 - \frac{4}{15}(1-\nu)\right\} a^2 \end{bmatrix} \tag{6.38}$$

and

$$\alpha = \frac{a}{b}, \qquad \beta = \frac{b}{a}. \tag{6.39}$$

Defining the following matrices

$$\mathbf{I}_1 = \begin{bmatrix} -1 & 0 & 0 \\ 0 & 1 & 0 \\ 0 & 0 & 1 \end{bmatrix}, \qquad \mathbf{I}_2 = \begin{bmatrix} 1 & 0 & 0 \\ 0 & -1 & 0 \\ 0 & 0 & 1 \end{bmatrix}, \qquad \mathbf{I}_3 = \begin{bmatrix} 1 & 0 & 0 \\ 0 & 1 & 0 \\ 0 & 0 & -1 \end{bmatrix} \tag{6.40}$$

the remaining sub-matrices of (6.34) are given by

$$\begin{aligned} &\mathbf{k}_{22} = \mathbf{I}_3^{\mathrm{T}} \mathbf{k}_{11} \mathbf{I}_3 \\ &\mathbf{k}_{32} = \mathbf{I}_3^{\mathrm{T}} \mathbf{k}_{41} \mathbf{I}_3, \qquad \mathbf{k}_{33} = \mathbf{I}_1^{\mathrm{T}} \mathbf{k}_{11} \mathbf{I}_1 \\ &\mathbf{k}_{42} = \mathbf{I}_3^{\mathrm{T}} \mathbf{k}_{31} \mathbf{I}_3, \qquad \mathbf{k}_{43} = \mathbf{I}_1^{\mathrm{T}} \mathbf{k}_{21} \mathbf{I}_1, \qquad \mathbf{k}_{44} = \mathbf{I}_2^{\mathrm{T}} \mathbf{k}_{11} \mathbf{I}_2 \end{aligned} \tag{6.41}$$

These relationships are derived in reference [6.3].

As in the case of the inertia matrix, it is simpler to use the expression (6.8) for w and substitute for $\{\boldsymbol{\alpha}\}$ after performing the integration using (6.30). This procedure has been generalised for a number of plate elements with anisotropic material properties in reference [6.4].

Substituting (6.17) into (6.4) gives

$$\delta W_e = \{\delta \mathbf{w}\}_e^{\mathrm{T}} \{\mathbf{f}\}_e \tag{6.42}$$

where

$$\{\mathbf{f}\}_e = \int_A \lfloor \mathbf{N} \rfloor^{\mathrm{T}} p_z \, \mathrm{d}A \tag{6.43}$$

https://doi.org/10.1017/CBO9780511761195.008 Published online by Cambridge University Press

is the element equivalent nodal force matrix. Assuming p_z to be constant, substituting for $\lfloor \mathbf{N} \rfloor$ from (6.19) and integrating gives

$$\{\mathbf{f}\}_e = p_z \frac{ab}{3} \begin{bmatrix} 3 \\ b \\ -a \\ 3 \\ b \\ a \\ 3 \\ -b \\ a \\ 3 \\ -b \\ -a \end{bmatrix} \tag{6.44}$$

The stresses at any point in the plate are given by (2.63)

$$\begin{bmatrix} \sigma_x \\ \sigma_y \\ \tau_{xy} \end{bmatrix} = \{\boldsymbol{\sigma}\} = [\mathbf{D}]\{\boldsymbol{\varepsilon}\} \tag{6.45}$$

Substituting for the strains $\{\boldsymbol{\varepsilon}\}$ from (2.65) gives

$$\{\boldsymbol{\sigma}\} = -z[\mathbf{D}]\{\boldsymbol{\chi}\} \tag{6.46}$$

where $\{\boldsymbol{\chi}\}$ is defined in (6.3). Substituting for w in $\{\boldsymbol{\chi}\}$ using (6.17) gives

$$\{\boldsymbol{\sigma}\} = -z[\mathbf{D}][\mathbf{B}]\{\mathbf{w}\}_e \tag{6.47}$$

where $[\mathbf{B}]$ is defined in (6.33) and $\{\mathbf{w}\}_e$ in (6.18). Since $[\mathbf{B}]$ is a function of x and y (or ξ and η), then (6.47) gives the stresses at the point (x, y, z) in terms of the nodal displacements.

The bending moments M_x and M_y and twisting moments M_{xy} and M_{yx} per unit length are defined by

$$\begin{aligned} M_x &= \int_{-h/2}^{+h/2} \sigma_x z \, \mathrm{d}z, & M_y &= \int_{-h/2}^{+h/2} \sigma_y z \, \mathrm{d}z \\ M_{xy} &= -\int_{-h/2}^{+h/2} \tau_{xy} z \, \mathrm{d}z, & M_{yx} &= \int_{-h/2}^{+h/2} \tau_{yx} z \, \mathrm{d}z \end{aligned} \tag{6.48}$$

Since $\tau_{yx} = \tau_{xy}$ then $M_{yx} = -M_{xy}$. The directions of these moments are indicated in Figure 6.2.

Substituting (6.47) into (6.48) and integrating gives

$$\begin{bmatrix} M_x \\ M_y \\ M_{xy} \end{bmatrix} = -\frac{h^3}{12}[\mathbf{I}]_3[\mathbf{D}][\mathbf{B}]\{\mathbf{w}\}_e \tag{6.49}$$

where $[\mathbf{I}]_3$ is defined in (6.40).

https://doi.org/10.1017/CBO9780511761195.008 Published online by Cambridge University Press

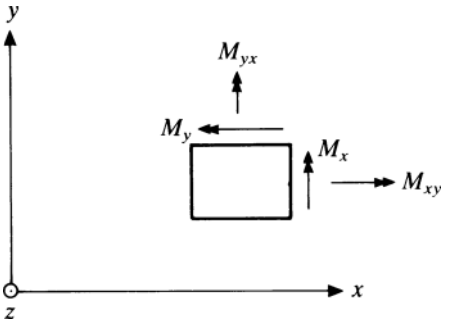

Figure 6.2. Sign convention for bending and twisting moments.

Both bending moments and stresses will be more accurate at a (2×2) array of integration points.

EXAMPLE 6.1 Use the ACM element to estimate the five lowest frequencies of a square plate which is simply supported on all four edges. Compare the results with the analytical solution $\pi^2(m^2 + n^2)(D/\rho h L^4)^{1/2}$ rad/s, where L is the length of each side and (m, n) are the number of half-waves in the x- and y-directions.

Since the plate has two axes of symmetry, the modes which are symmetric or antisymmetric about each of these can be calculated separately by idealising one-quarter of the plate and applying appropriate boundary conditions on the axes of symmetry (Chapter 8).

Figure 6.3 shows one-quarter of the plate represented by four rectangular elements. Since side 1–3 is simply supported w, θ_y are zero at nodes 1, 2 and 3. Similarly, since side 1–7 is simply supported w, θ_x are zero at nodes 1, 4 and 7. The modes which are symmetric with respect to the side 3–9 are obtained by setting θ_y zero at 3, 6 and 9, and the antisymmetric modes by setting w, θ_x to be zero at 3, 6 and 9. Similarly, the modes which are symmetric with respect to the side 7–9 are obtained by setting θ_x to be zero at 7, 8 and 9, and the antisymmetric modes by setting w, θ_y to be zero at 7, 8 and 9. Therefore, the modes which are symmetric with respect to both axes of symmetry are obtained by considering a twelve degree of freedom model, the degrees of freedom being w at 9, θ_x at 2 and 3, θ_y at 4 and 7, w and θ_x at 6, w and θ_y at 8, and w, θ_x, θ_y at 5.

Analyses have been performed using (2×2), (3×3), (4×4) and (5×5) meshes of elements for the quarter plate. The results are compared with the analytical frequencies in Figure 6.4. Unlike the examples presented in the

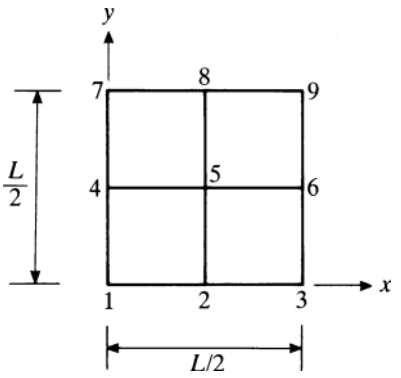

Figure 6.3. Idealisation of one-quarter of a square plate.

https://doi.org/10.1017/CBO9780511761195.008 Published online by Cambridge University Press

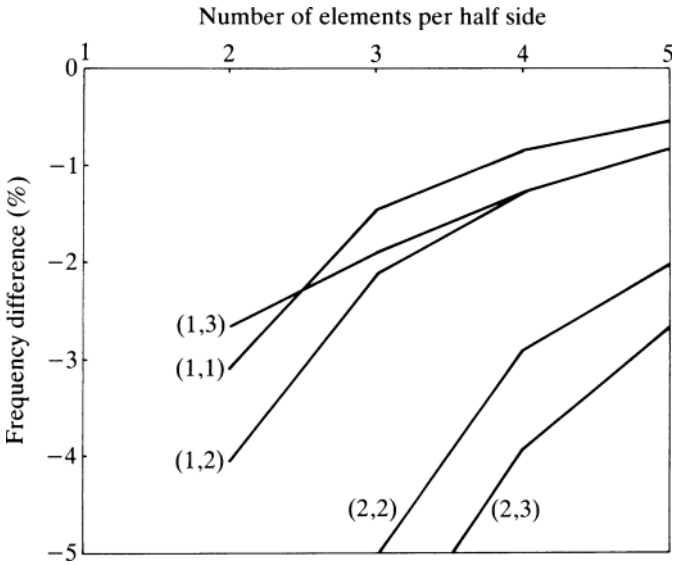

Figure 6.4. Flexural vibrations of a simply supported square plate. ACM element.

previous chapters, the frequencies predicted using the finite element method are less than the analytical frequencies. This is a consequence of the ACM element being a non-conforming one. However, as can be seen from the figure, this does not preclude the frequencies from converging to the analytical frequencies as the number of elements is increased. Results for a variety of other boundary conditions are presented in references [6.5, 6.6].

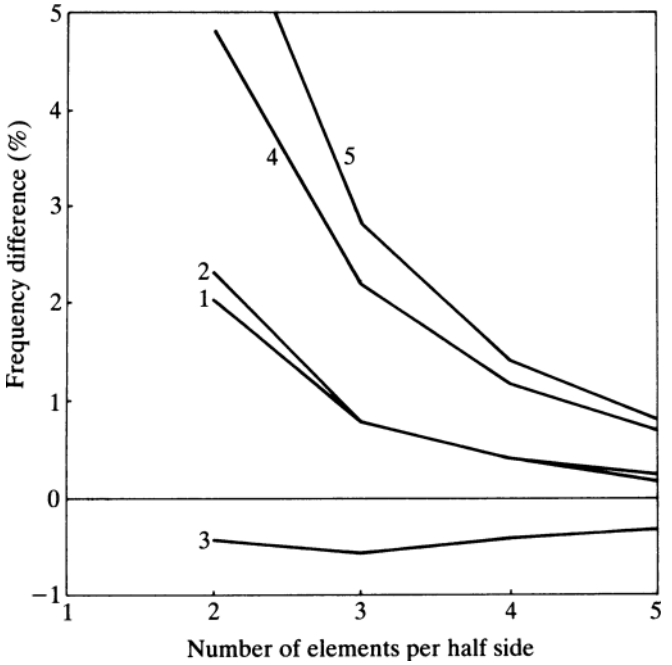

Figure 6.5. Flexural vibrations of a simply supported/free square plate. ACM element.

https://doi.org/10.1017/CBO9780511761195.008 Published online by Cambridge University Press

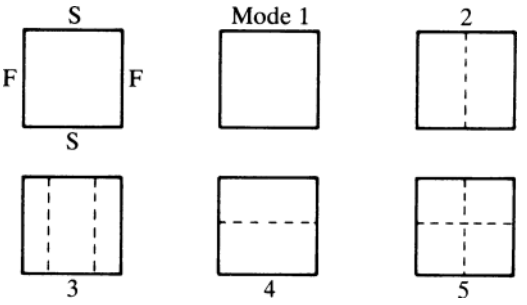

Figure 6.6. Modal patterns for a simply supported (S)/free (F) square plate.

It cannot be asserted that frequencies predicted by the ACM element will always be less than the correct ones. In fact, predictions can be either above or below the true ones. This is illustrated by the results for a square plate having one pair of opposite sides simply supported and the other pair free, as shown in Figure 6.5. The modal patterns are illustrated in Figure 6.6. Four of the five modes shown converge from above whilst the other converges from below.

EXAMPLE 6.2 Calculate the first six natural frequencies and modes of a square plate of side 0.3048 m and thickness 3.2766 mm which is point supported at its four corners. Compare the results with the analytical solutions given in references [6.8, 6.9] and the experimental results of [6.7]. Take $E = 73.084 \times 10^9$ N/m^2, $\nu = 0.3$, $\rho = 2821$ kg/m^3.

The plate has two axes of symmetry. A quarter plate was therefore represented by (2×2) and (4×4) meshes of elements. Either symmetric or antisymmetric boundary conditions were applied along the axes of symmetry. In addition, the displacement w at the corner node point was set to zero.

The predicted frequencies are compared with the analytical and experimental ones in Table 6.1. The modal patterns are given in Figure 6.7. Notice that there are two modes with different modal patterns 2(a) and 2(b) having identical frequencies.

EXAMPLE 6.3 Figure 6.8(a) shows a rectangular plate which is stiffened in one direction. The details of the stiffener are given in Figure 6.8(b). Calculate the frequencies of the first four modes by considering an equivalent orthotropic

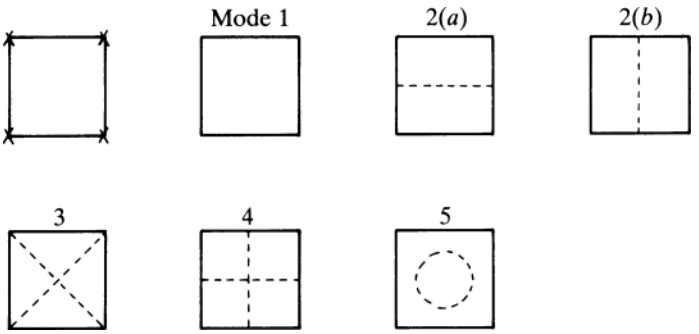

Figure 6.7. Modal patterns for a corner supported square plate.

https://doi.org/10.1017/CBO9780511761195.008 Published online by Cambridge University Press

Table 6.1. *Comparison of predicted frequencies of a corner supported square plate. ACM element*

	FEM [6.9]		Analytical		Experimental
Mode	(2 × 2)	(4 × 4)	[6.7]	[6.8]	[6.7]
1	62.15	62.09	61.4	61.11	62
2(*a*), (*b*)	141.0	138.5	136	134.6	134
3	169.7	169.7	170	166.3	169
4	343.7	340.0	333	331.9	330
5	397.4	396.0	385	383.1	383

plate and assuming all four edges to be simply supported. Compare the results with the analytical solutions given in reference [6.10]. Take $E = 206.84 \times 10^9$ N/m^2, $\nu = 0.3$ and $\rho = 7833$ kg/m^3.

The material axes, $\bar{x}$, $\bar{y}$, of the equivalent orthotropic plate are coincident with the geometric axes, x, y, shown in Figure 6.8(a). Using the method given in reference [6.11] the elastic constants of this equivalent plate are

$$D_x = 3.396D, \qquad D_y = D, \qquad H = 1.08D$$

where

$$D_x = \frac{E'_x h_e^3}{12}, \qquad D_y = \frac{E'_y h_e^3}{12}$$

$$H = \frac{E'_x \nu_{xy} h_e^3}{12} + \frac{G_{xy} h_e^3}{6}$$

$$D = \frac{Eh^3}{12(1-\nu^2)}$$

h = thickness of unstiffened plate

h_e = thickness of equivalent orthotropic plate

$= 1.125h$

E'_x, E'_y ν_{xy} are defined in Chapter 2

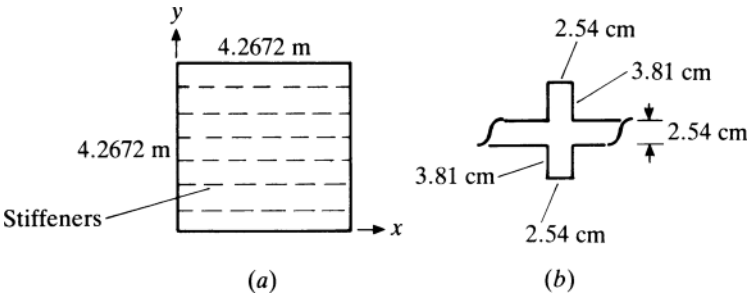

Figure 6.8. Geometry of a stiffened square plate.

https://doi.org/10.1017/CBO9780511761195.008 Published online by Cambridge University Press

Table 6.2. *Comparison of predicted frequencies of a stiffened, simply supported plate*

	Analytical (Hz) [6.10]		
Mode	Discrete	Smeared	FEM (ACM)
(1, 1)	8.089	8.258	8.142
(1, 2)	16.720	17.092	16.721
(2, 1)	25.249	25.824	25.373
(2, 2)	32.357	33.067	31.631

Using the values of E, ν and ρ given and the above relationships, it can be shown that the material properties of the equivalent orthotropic plate are:

$$E_x = 493.313 \times 10^9 \text{ N/m}^2$$
$$E_y = 145.266 \times 10^9 \text{ N/m}^2$$
$$\nu_{xy} = 0.1628$$
$$G_{xy} = 42.072 \times 10^9 \text{ N/m}^2$$
$$\rho = 7833 \text{ kg/m}^3$$
$$h_e = 2.8575 \text{ cm}$$

The full plate was analysed using an (8×8) mesh of elements. This means that there were 81 node points with three degrees of freedom each. Of the 243 degrees of freedom, 68 are zero due to the simply supported boundary conditions. Seventy-seven master degrees of freedom (see Chapter 11) were then selected automatically from the remaining 175 degrees of freedom. The frequencies obtained are given in Table 6.2. These are compared with two sets of analytically predicted frequencies. The first set was obtained by treating the plate as a discretely stiffened plate. The second set was obtained by considering the equivalent orthotropic plate and using the Rayleigh method.

It has been indicated that the element presented in this section is a non-conforming one, since the normal slope is not continuous between elements. There are several ways of overcoming this problem, namely:

(1) Introduce additional nodal degrees of freedom.
(2) Ensure that the normal slope varies linearly along an edge.
(3) Introduce additional node points.
(4) Use thick plate theory and reduced integration (see Section 3.10 for a similar treatment of a beam).

These methods will be presented in the following sections.

6.2 Thin Rectangular Element (conforming)

A conforming rectangular element can be obtained by taking products of the functions (3.126) for a uniform, slender beam. In this case the displacement function for

https://doi.org/10.1017/CBO9780511761195.008 Published online by Cambridge University Press

the plate is of the form (6.17) with

$$\mathbf{N}_j^{\mathrm{T}}(\xi,\eta)=\begin{bmatrix} f_j(\xi)\,f_j(\eta) \\ bf_j(\xi)g_j(\eta) \\ -ag_j(\xi)\,f_j(\eta) \end{bmatrix} \tag{6.50}$$

where

$$f_j(\xi)=\tfrac{1}{4}(2+3\xi_j\xi-\xi_j\xi^3)$$

and

$$g_j(\xi)=\tfrac{1}{4}(-\xi_j-\xi+\xi_j\xi^2+\xi^3) \tag{6.51}$$

The functions of η are obtained by replacing ξ_j, ξ by η_j, η respectively. (ξ_j, η_j) are the coordinates of node j.

A close inspection of the displacement function defined by (6.17), (6.50) and (6.51) reveals that the twist $\partial^2 w/\partial x\partial y$ is zero at the four node points. This means that, in the limit, as an increasing number of elements is used, the plate will tend towards a zero twist condition. This can be overcome by introducing $\partial^2 w/\partial x\partial y$ as an additional degree of freedom at each node point. In this case the displacement function is of the form (6.17) with

$$\{\mathbf{w}\}_e^{\mathrm{T}}=\lfloor w_1 \quad \theta_{x1} \quad \theta_{y1} \quad w_{xy1} \quad \cdots \quad w_4 \quad \theta_{x4} \quad \theta_{y4} \quad w_{xy4}\rfloor \tag{6.52}$$

where $w_{xy}\equiv \partial^2 w/\partial x\,\partial y$, and

$$\mathbf{N}_j^{\mathrm{T}}(\xi,\eta)=\begin{bmatrix} f_j(\xi)\,f_j(\eta) \\ bf_j(\xi)g_j(\eta) \\ -ag_j(\xi)\,f_j(\eta) \\ abg_j(\xi)g_j(\eta) \end{bmatrix} \tag{6.53}$$

This element is commonly referred to as the CR element [6.12].

By specifying nodal degrees of freedom which are consistent with rigid body displacements, corresponding to vertical translation and rotation about the x- and y-axes, it can be shown that this element can perform rigid body movement without deformation. Similarly for pure bending in the x- and y-directions. (Note that this is also true for the functions (6.50).) The nodal displacements which are consistent with a state of constant twist are

$$\begin{aligned} w_1, w_3 &= 1, & w_2, w_4 &= -1 \\ \theta_{x2}, \theta_{x3} &= \frac{1}{b}, & \theta_{x1}, \theta_{x4} &= -\frac{1}{b} \\ \theta_{y1}, \theta_{y2} &= \frac{1}{a}, & \theta_{y3}, \theta_{y4} &= -\frac{1}{a} \\ w_{xyj} &= \frac{1}{ab}, & j &= 1,\ldots,4. \end{aligned} \tag{6.54}$$

Substituting these into (6.17) and (6.53) gives

$$w=\xi\eta \tag{6.55}$$

as required. Thus, the first six terms in (6.5) are present in the functions (6.53).

https://doi.org/10.1017/CBO9780511761195.008 Published online by Cambridge University Press

The element inertia, stiffness and equivalent nodal force matrices are given by (6.25), (6.32) and (6.43) where the matrix $\lfloor \mathbf{N} \rfloor$ is defined by (6.17) and (6.53). These expressions may be evaluated by the combined analytical/numerical method given in reference [6.4]. They can also be evaluated analytically. The burden of the calculations is considerably eased if the functions (6.51) are expressed in terms of Legendre polynomials [6.13] as follows:

$$\begin{aligned} f_j(\xi) &= \tfrac{1}{2}P_0 + \tfrac{3}{5}\xi_j P_1 - \tfrac{1}{10}\xi_j P_3 \\ g_j(\xi) &= -\tfrac{1}{6}\xi_j P_0 - \tfrac{1}{10}P_1 + \tfrac{1}{6}\xi_j P_2 + \tfrac{1}{10}P_3 \end{aligned} \tag{6.56}$$

where

$$\begin{aligned} &P_0 = 1, \qquad P_1 = \xi, \qquad P_2 = \tfrac{1}{2}(3\xi^2 - 1), \\ &P_3 = \tfrac{1}{2}(5\xi^3 - 3\xi) \end{aligned} \tag{6.57}$$

(see Section 3.10 for further details).

The derivatives of these functions can also be expressed in terms of Legendre polynomials, viz:

$$\begin{aligned} f_j'(\xi) &= \tfrac{1}{2}\xi_j P_0 - \tfrac{1}{2}\xi_j P_2 \\ f_j''(\xi) &= -\tfrac{3}{2}\xi_j P_1 \\ g_j'(\xi) &= \tfrac{1}{2}\xi_j P_1 + P_2 \\ g_j''(\xi) &= \tfrac{1}{2}\xi_j P_0 + \tfrac{3}{2}P_1 \end{aligned} \tag{6.58}$$

Integrals of products of the functions (6.51) and their derivatives can now be evaluated using the following relationships:

$$\int_{-1}^{+1} P_n(\xi) P_m(\xi)\, \mathrm{d}\xi = \begin{cases} \dfrac{2}{(2n+1)} & \text{when } m = n \\ 0 & \text{when } m \neq n \end{cases} \tag{6.59}$$

All three matrices are presented in reference [6.12] and the stiffness matrix in [6.13], both for the isotropic case. The extension to the orthotropic case can be found in reference [6.14].

EXAMPLE 6.4 Repeat Example 6.1 using the CR element.

The boundary conditions along a simply supported edge are the same as in Example 6.1 since $w_{xy} \neq 0$ there. Along an axis of symmetry the boundary conditions are the same as in Example 6.1 for antisymmetric modes, but in the case of symmetric modes there is the additional constraint that w_{xy} is zero.

The percentage differences between the finite element and analytical frequencies are presented in Table 6.3. The accuracy of this element is considerably better than the accuracy obtained with the ACM element (see Figure 6.5). In fact the present results would be insignificant if drawn on the same scale as the figure. Also, note that the CR element produces frequencies which are greater than the exact analytical frequencies. This is because all the requirements of the Rayleigh-Ritz method have been satisfied (see Section 3.1). Results for a variety of boundary conditions are presented in references [6.5, 6.6, 6.15 and 6.16].

https://doi.org/10.1017/CBO9780511761195.008 Published online by Cambridge University Press

Table 6.3. *Comparison of predicted and analytical frequencies for a simply supported square plate. CR element (% difference)*

	FEM grids ($\frac{1}{4}$ plate)			
Mode	2×2	3×3	4×4	5×5
(1, 1)	0.02	0.01	0.0	0.0
(1, 2), (2, 1)	0.26	0.05	0.02	0.01
(2, 2)	0.22	0.04	0.01	0.01
(1, 3), (3, 1)	1.51	0.32	0.11	0.04
(2, 3), (3, 2)	0.99	0.21	0.07	0.03

EXAMPLE 6.5 Repeat Example 6.2 using the CR element.

The analysis is exactly the same as in Example 6.2 except there are now four degrees of freedom per node instead of three. Also, for modes which are symmetric about an axis of symmetry there is the additional constraint that w_{xy} is zero.

The predicted frequencies are compared with the analytical and experimental ones in Table 6.4. A comparison with Table 6.1 indicates that the frequencies predicted with the CR element are lower than the ones predicted with the ACM element.

Although the CR element is more accurate than the ACM element, it does suffer from the disadvantage that it is difficult to use in conjunction with other elements when analysing built-up structures (see Chapter 7) due to the presence of the degree of freedom w_{xy}. Because of this, reference [6.17] introduces the approximations

$$\begin{aligned} w_{xy1} &= \frac{1}{2b}(\theta_{y1} - \theta_{y4}), \qquad w_{xy2} = \frac{1}{2a}(\theta_{x2} - \theta_{x1}) \\ w_{xy3} &= \frac{1}{2b}(\theta_{y2} - \theta_{y3}), \qquad w_{xy4} = \frac{1}{2a}(\theta_{x3} - \theta_{x4}) \end{aligned} \tag{6.60}$$

Substituting (6.60) into (6.17), (6.52) and (6.53) and simplifying, shows that w is of the form (6.17) with $\{\mathbf{w}\}_e$ given by (6.18) and

$$\mathbf{N}_j^{\mathrm{T}} = (\xi, \eta) = \begin{bmatrix} f_j(\xi) f_j(\eta) \\ bF_j(\xi) g_j(\eta) \\ -ag_j(\xi) F_j(\eta) \end{bmatrix} \tag{6.61}$$

Table 6.4. *Comparison of predicted frequencies of a corner supported square plate*

	FEM [6.9] (CR)		Analytical		Experimental
Mode	(2×2)	(4×4)	[6.7]	[6.8]	[6.7]
1	62.03	61.79	61.4	62.11	62
2(a), (b)	138.9	134.9	136	134.6	134
3	169.7	169.6	170	166.3	169
4	338.9	335.1	333	331.9	330
5	391.5	387.5	385	383.1	383

https://doi.org/10.1017/CBO9780511761195.008 Published online by Cambridge University Press

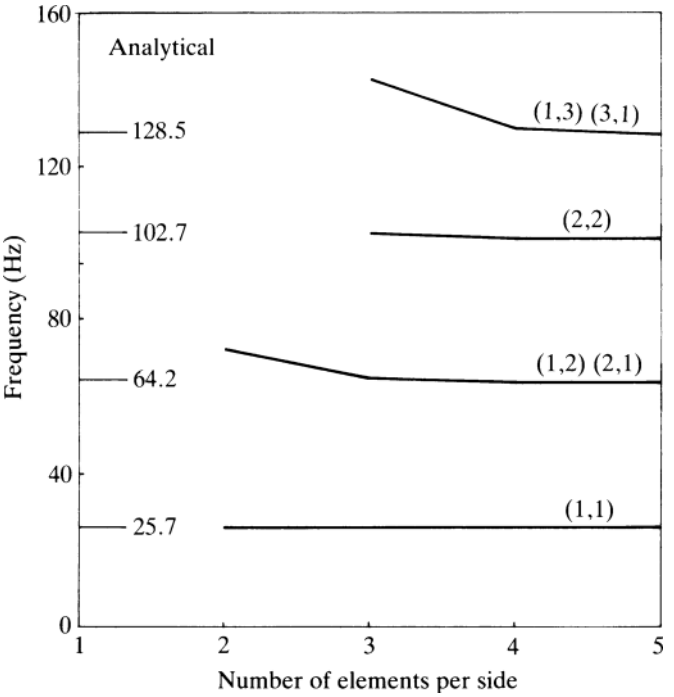

Figure 6.9. Flexural vibrations of a simply supported square plate. WB element [6.17].

where

$$F_j(\xi) = \begin{cases} \frac{1}{8}(5 + 5\xi_j\xi - \xi^2 - \xi_j\xi^3) & j = 1, 3 \\ \frac{1}{8}(3 + 5\xi_j\xi + \xi^2 - \xi_j\xi^3) & j = 2, 4 \end{cases} \tag{6.62}$$

and

$$F_j(\eta) = \begin{cases} \frac{1}{8}(3 + 5\eta_j\eta + \eta^2 - \eta_j\eta^3) & j = 1, 3 \\ \frac{1}{8}(5 + 5\eta_j\eta - \eta^2 - \eta_j\eta^3) & j = 2, 4 \end{cases} \tag{6.63}$$

(ξ_j, η_j) are the coordinates of node j. This element will be referred to as the WB element.

The effect of applying the constraints (6.60) to the CR element is to make it a non-conforming one. The displacement and tangential slope are continuous between elements but the normal slope is not.

EXAMPLE 6.6 Use the WB element to estimate the four lowest frequencies of a square plate of side 2.4 m and thickness 0.03 m, which is simply supported on all four edges. Take $E = 21 \times 10^{10}$ N/m^2, $\nu = 0.3$ and $\rho = 7800$ kg/m^3. Compare the results with the analytical solution $(\pi/2)(m^2 + n^2)(D/\rho h L^4)^{1/2}$ Hz, where L is the length of each side and (m, n) are the number of half-waves in the x- and y-directions.

The complete plate was represented by (2×2), (3×3), (4×4) and (5×5) meshes of elements. The frequencies obtained are presented in Figure 6.9. The frequencies obtained with the WB element rapidly converge to the analytical frequencies as the number of elements increases.

https://doi.org/10.1017/CBO9780511761195.008 Published online by Cambridge University Press

6.3 Thick Rectangular Element

The energy expressions for a thick plate element are, from Section 2.7

$$T_e = \frac{1}{2}\int_A \rho\left(h\dot{w}^2 + \frac{h^3}{12}\dot{\theta}_x^2 + \frac{h^3}{12}\dot{\theta}_y^2\right) \mathrm{d}A \tag{6.64}$$

$$U_e = \frac{1}{2}\int_A \frac{h^3}{12}\{\boldsymbol{\chi}\}^{\mathrm{T}}[\mathbf{D}]\{\boldsymbol{\chi}\}\,\mathrm{d}A + \frac{1}{2}\int_A \kappa h\{\boldsymbol{\gamma}\}^{\mathrm{T}}[\mathbf{D}^{\mathrm{s}}]\{\boldsymbol{\gamma}\}\,\mathrm{d}A \tag{6.65}$$

with

$$\{\boldsymbol{\chi}\} = \begin{bmatrix} -\partial\theta_y/\partial x \\ \partial\theta_x/\partial y \\ \partial\theta_x/\partial x - \partial\theta_y/\partial y \end{bmatrix}, \qquad \{\boldsymbol{\gamma}\} = \begin{bmatrix} \theta_y + \partial w/\partial x \\ -\theta_x + \partial w/\partial y \end{bmatrix} \tag{6.66}$$

where $[\mathbf{D}]$ is defined by (2.45), (2.49) or (2.51) and $[\mathbf{D}^{\mathrm{s}}]$ is defined by (2.77). Also

$$\delta W = \int_A p_z \delta w\,\mathrm{d}A \tag{6.67}$$

The highest derivative of w, θ_x and θ_y appearing in the energy expressions is the first. Therefore, w, θ_x and θ_y are the only degrees of freedom required at the node points. The displacement functions are of the form

$$w = \sum_{j=1}^{4} N_j w_j, \qquad \theta_x = \sum_{j=1}^{4} N_j \theta_{x_i}, \qquad \theta_y = \sum_{j=1}^{4} N_j \theta_{y_i} \tag{6.68}$$

where the functions N_j are defined by (4.36), that is

$$N_j = \tfrac{1}{4}(1 + \xi_j\xi)(1 + \eta_j\eta) \tag{6.69}$$

These functions ensure that w, θ_x and θ_y are continuous between elements. This element will be referred to as the HTK element [6.18]. Combining the expressions (6.68) gives

$$\begin{bmatrix} w \\ \theta_x \\ \theta_y \end{bmatrix} = [\mathbf{N}]\{\mathbf{w}\}_e \tag{6.70}$$

where

$$\{\mathbf{w}\}_e^{\mathrm{T}} = \lfloor w_1 \quad \theta_{x1} \quad \theta_{y1} \quad \cdots \quad w_4 \quad \theta_{x4} \quad \theta_{y4} \rfloor \tag{6.71}$$

and

$$[\mathbf{N}] = \begin{bmatrix} N_1 & 0 & 0 & \cdots & N_4 & 0 & 0 \\ 0 & N_1 & 0 & \cdots & 0 & N_4 & 0 \\ 0 & 0 & N_1 & \ldots & 0 & 0 & N_4 \end{bmatrix} \tag{6.72}$$

Substituting (6.70) into (6.64) gives

$$T_e = \tfrac{1}{2}\{\dot{\mathbf{w}}\}_e^{\mathrm{T}}[\mathbf{m}]_e\{\dot{\mathbf{w}}\}_e \tag{6.73}$$

https://doi.org/10.1017/CBO9780511761195.008 Published online by Cambridge University Press

where

$$[\mathbf{m}]_e = \int_A \rho\,[\mathbf{N}]^{\mathrm{T}} \begin{bmatrix} h & 0 & 0 \\ 0 & h^3/12 & 0 \\ 0 & 0 & h^3/12 \end{bmatrix} [\mathbf{N}]\,\mathrm{d}A \tag{6.74}$$

Substituting the functions (6.69) into (6.74) and integrating gives

$$[\mathbf{m}]_e = [\mathbf{m}^{\mathrm{t}}] + [\mathbf{m}^{\mathrm{r}}] \tag{6.75}$$

where

$$[\mathbf{m}^{\mathrm{t}}] = \frac{\rho hab}{108} \begin{bmatrix} 48 & & & & & & & & & & & \\ 0 & 0 & & & & & & & & \text{Sym} & & \\ 0 & 0 & 0 & & & & & & & & & \\ 24 & 0 & 0 & 48 & & & & & & & & \\ 0 & 0 & 0 & 0 & 0 & & & & & & & \\ 0 & 0 & 0 & 0 & 0 & 0 & & & & & & \\ 12 & 0 & 0 & 24 & 0 & 0 & 48 & & & & & \\ 0 & 0 & 0 & 0 & 0 & 0 & 0 & 0 & & & & \\ 0 & 0 & 0 & 0 & 0 & 0 & 0 & 0 & 0 & & & \\ 24 & 0 & 0 & 12 & 0 & 0 & 24 & 0 & 0 & 48 & & \\ 0 & 0 & 0 & 0 & 0 & 0 & 0 & 0 & 0 & 0 & 0 & \\ 0 & 0 & 0 & 0 & 0 & 0 & 0 & 0 & 0 & 0 & 0 & 0 \end{bmatrix} \tag{6.76}$$

$$[\mathbf{m}^{\mathrm{r}}] = \frac{\rho h^3 ab}{108} \begin{bmatrix} 0 & & & & & & & & & & & \\ 0 & 4 & & & & & & & & \text{Sym} & & \\ 0 & 0 & 4 & & & & & & & & & \\ 0 & 0 & 0 & 0 & & & & & & & & \\ 0 & 2 & 0 & 0 & 4 & & & & & & & \\ 0 & 0 & 2 & 0 & 0 & 4 & & & & & & \\ 0 & 0 & 0 & 0 & 0 & 0 & 0 & & & & & \\ 0 & 1 & 0 & 0 & 2 & 0 & 0 & 4 & & & & \\ 0 & 0 & 1 & 0 & 0 & 2 & 0 & 0 & 4 & & & \\ 0 & 0 & 0 & 0 & 0 & 0 & 0 & 0 & 0 & 0 & & \\ 0 & 2 & 0 & 0 & 1 & 0 & 0 & 2 & 0 & 0 & 4 & \\ 0 & 0 & 2 & 0 & 0 & 1 & 0 & 0 & 2 & 0 & 0 & 4 \end{bmatrix} \tag{6.77}$$

Substituting (6.70) into (6.66) and (6.65) gives

$$U_e = \tfrac{1}{2}\{\mathbf{w}\}_e^{\mathrm{T}}[\mathbf{k}]_e\{\mathbf{w}\}_e \tag{6.78}$$

where the stiffness matrix $[\mathbf{k}]_e$ is of the form

$$[\mathbf{k}]_e = [\mathbf{k}^{\mathrm{f}}] + [\mathbf{k}^{\mathrm{s}}] \tag{6.79}$$

https://doi.org/10.1017/CBO9780511761195.008 Published online by Cambridge University Press

where

$$[\mathbf{k}^{\mathrm{f}}] = \int_A \frac{h^3}{12}[\mathbf{B}^{\mathrm{f}}]^{\mathrm{T}}\,[\mathbf{D}]\,[\mathbf{B}^{\mathrm{f}}]\,\mathrm{d}A \tag{6.80}$$

and

$$[\mathbf{k}^{\mathrm{s}}] = \int_A \kappa h[\mathbf{B}^{\mathrm{s}}]^{\mathrm{T}}\,[\mathbf{D}^{\mathrm{s}}]\,[\mathbf{B}^{\mathrm{s}}]\,\mathrm{d}A \tag{6.81}$$

The strain matrix $[\mathbf{B}^{\mathrm{f}}]$ is of the form

$$[\mathbf{B}^{\mathrm{f}}] = [\mathbf{B}^{\mathrm{f}}_1 \quad \mathbf{B}^{\mathrm{f}}_2 \quad \mathbf{B}^{\mathrm{f}}_3 \quad \mathbf{B}^{\mathrm{f}}_4] \tag{6.82}$$

where

$$\mathbf{B}^{\mathrm{f}}_j = \begin{bmatrix} 0 & 0 & -\partial N_j/\partial x \\ 0 & \partial N_j/\partial y & 0 \\ 0 & \partial N_j/\partial x & -\partial N_j/\partial y \end{bmatrix} \tag{6.83}$$

The strain matrix $[\mathbf{B}^{\mathrm{s}}]$ is of the form

$$[\mathbf{B}^{\mathrm{s}}] = [\mathbf{B}^{\mathrm{s}}_1 \quad \mathbf{B}^{\mathrm{s}}_2 \quad \mathbf{B}^{\mathrm{s}}_3 \quad \mathbf{B}^{\mathrm{s}}_4] \tag{6.84}$$

where

$$\mathbf{B}^{\mathrm{s}}_j = \begin{bmatrix} \partial N_j/\partial x & 0 & N_j \\ \partial N_j/\partial y & -N_j & 0 \end{bmatrix} \tag{6.85}$$

Substituting (6.69) into (6.83) and (6.85) gives

$$\mathbf{B}^{\mathrm{f}}_j = \begin{bmatrix} 0 & 0 & -\xi_j(1+\eta_j\eta)/4a \\ 0 & (1+\xi_j\xi)\eta_j/4b & 0 \\ 0 & \xi_j(1+\eta_j\eta)/4a & -(1+\xi_j\xi)\eta_j/4b \end{bmatrix} \tag{6.86}$$

and

$$\mathbf{B}^{\mathrm{s}}_j = \begin{bmatrix} \xi_j(1+\eta_j\eta)/4a & 0 & (1+\xi_j\xi)(1+\eta_j\eta)/4 \\ (1+\xi_j\xi)\eta_j/4b & -(1+\xi_j\xi)(1+\eta_j\eta)/4 & 0 \end{bmatrix} \tag{6.87}$$

Substituting (6.86) and (6.87) into (6.82) and (6.84) and the resulting matrices into (6.80) and (6.81) will give the element stiffness matrix as defined by (6.79). Both (6.80) and (6.81) may be evaluated exactly using a (2×2) array of Gauss integration points. For thick plates this gives acceptable results. However, as the thickness of the plate is reduced, the element becomes over-stiff in the same way as the corresponding deep beam formulation discussed in Sections 3.9 and 3.10. This can be overcome by evaluating the shear energy term (6.81) using a one point Gauss integration scheme [6.18, 6.19].

For the isotropic case, the stiffness matrix due to flexure is of the form

$$[\mathbf{k}^{\mathrm{f}}] = \frac{Eh^3}{48ab(1-\nu)^2} \begin{bmatrix} \mathbf{k}^{\mathrm{f}}_{11} & & & \mathrm{Sym} \\ \mathbf{k}^{\mathrm{f}}_{21} & \mathbf{k}^{\mathrm{f}}_{22} & & \\ \mathbf{k}^{\mathrm{f}}_{31} & \mathbf{k}^{\mathrm{f}}_{32} & \mathbf{k}^{\mathrm{f}}_{33} & \\ \mathbf{k}^{\mathrm{f}}_{41} & \mathbf{k}^{\mathrm{f}}_{42} & \mathbf{k}^{\mathrm{f}}_{43} & \mathbf{k}^{\mathrm{f}}_{44} \end{bmatrix} \tag{6.88}$$

https://doi.org/10.1017/CBO9780511761195.008 Published online by Cambridge University Press

where

$$\mathbf{k}_{11}^{\mathrm{f}} = \begin{bmatrix} 0 & 0 & 0 \\ 0 & \frac{4}{3}\left\{\alpha^2 + \frac{1}{2}(1-\nu)\right\} b^2 & -\frac{1}{2}(1+\nu)ab \\ 0 & -\frac{1}{2}(1+\nu)ab & \frac{4}{3}\left\{\beta^2 + \frac{1}{2}(1-\nu)\right\} a^2 \end{bmatrix} \tag{6.89}$$

$$\mathbf{k}_{21}^{\mathrm{f}} = \begin{bmatrix} 0 & 0 & 0 \\ 0 & \frac{2}{3}\left\{\alpha^2 - (1-\nu)\right\} b^2 & -\frac{1}{2}(3\nu-1)ab \\ 0 & \frac{1}{2}(3\nu-1)ab & \frac{1}{3}\left\{-4\beta^2 + (1-\nu)\right\} a^2 \end{bmatrix} \tag{6.90}$$

$$\mathbf{k}_{31}^{\mathrm{f}} = \begin{bmatrix} 0 & 0 & 0 \\ 0 & \frac{2}{3}\left\{-\alpha^2 - \frac{1}{2}(1-\nu)\right\} b^2 & \frac{1}{2}(1+\nu)ab \\ 0 & \frac{1}{2}(1+\nu)ab & \frac{2}{3}\left\{-\beta^2 - \frac{1}{2}(1-\nu)\right\} a^2 \end{bmatrix} \tag{6.91}$$

$$\mathbf{k}_{41}^{\mathrm{f}} = \begin{bmatrix} 0 & 0 & 0 \\ 0 & \frac{1}{3}\left\{-4\alpha^2 + (1-\nu)\right\} b^2 & \frac{1}{2}(3\nu-1)ab \\ 0 & -\frac{1}{2}(3\nu-1)ab & \frac{2}{3}\left\{\beta^2 - (1-\nu)\right\} a^2 \end{bmatrix} \tag{6.92}$$

and

$$\alpha = \frac{a}{b}, \qquad \beta = \frac{b}{a} \tag{6.93}$$

The remaining sub-matrices of (6.88) are given by relationships corresponding to (6.41).

The stiffness matrix due to shear is of the form

$$[\mathbf{k}^{\mathrm{s}}] = \frac{Eh^3}{48ab\beta_{\mathrm{s}}} \begin{bmatrix} \mathbf{k}_{11}^{\mathrm{s}} & & & \\ \mathbf{k}_{21}^{\mathrm{s}} & \mathbf{k}_{22}^{\mathrm{s}} & & \mathrm{Sym} \\ \mathbf{k}_{31}^{\mathrm{s}} & \mathbf{k}_{32}^{\mathrm{s}} & \mathbf{k}_{33}^{\mathrm{s}} & \\ \mathbf{k}_{41}^{\mathrm{s}} & \mathbf{k}_{42}^{\mathrm{s}} & \mathbf{k}_{43}^{\mathrm{s}} & \mathbf{k}_{44}^{\mathrm{s}} \end{bmatrix} \tag{6.94}$$

where $\beta_{\mathrm{s}} = Eh^2/12\kappa Gb^2$ is a shear parameter which is similar to the one defined in Sections 3.9 and 3.10 for a deep beam, also

$$\mathbf{k}_{11}^{\mathrm{s}} = \begin{bmatrix} (1+\alpha^2) & \alpha^2 b & -a \\ \alpha^2 b & \alpha^2 b^2 & 0 \\ -a & 0 & a^2 \end{bmatrix} \tag{6.95}$$

$$\mathbf{k}_{21}^{\mathrm{s}} = \begin{bmatrix} (-1+\alpha^2) & \alpha^2 b & a \\ \alpha^2 b & \alpha^2 b^2 & 0 \\ -a & 0 & a^2 \end{bmatrix} \tag{6.96}$$

https://doi.org/10.1017/CBO9780511761195.008 Published online by Cambridge University Press

$$\mathbf{k}_{31}^{s} = \begin{bmatrix} (-1-\alpha^2) & -\alpha^2 b & a \\ \alpha^2 b & \alpha^2 b & 0 \\ -a & 0 & a^2 \end{bmatrix} \tag{6.97}$$

$$\mathbf{k}_{41}^{s} = \begin{bmatrix} (1-\alpha^2) & -\alpha^2 b & -a \\ \alpha^2 b & \alpha^2 b^2 & 0 \\ -a & 0 & a^2 \end{bmatrix} \tag{6.98}$$

The remaining sub-matrices of (6.94) are given by relationships corresponding to (6.41).

Substituting for w from (6.68) into (6.67) gives

$$\delta W_e = \{\delta \mathbf{w}\}_e^{\mathrm{T}} \{\mathbf{f}\}_e \tag{6.99}$$

where

$$\{\mathbf{f}\}_e = \int_A [\mathbf{N}]^{\mathrm{T}} \begin{bmatrix} p_z \\ 0 \\ 0 \end{bmatrix} \mathrm{d}A \tag{6.100}$$

is the element equivalent nodal force matrix. Assuming p_z to be constant, substituting for $[\mathbf{N}]$ from (6.72) and (6.69) and integrating gives

$$\{\mathbf{f}\}_e = p_z ab \begin{bmatrix} 1 \\ 0 \\ 0 \\ 1 \\ 0 \\ 0 \\ 1 \\ 0 \\ 0 \\ 1 \\ 0 \\ 0 \end{bmatrix} \tag{6.101}$$

In this case one quarter of the total force is concentrated at each node.

The bending and twisting moments within the element are, from (6.49),

$$\begin{bmatrix} M_x \\ M_y \\ M_{xy} \end{bmatrix} = -\frac{h^3}{12} [\mathbf{I}]_3 [\mathbf{D}] [\mathbf{B}^{\mathrm{f}}] \{\mathbf{w}\}_e \tag{6.102}$$

https://doi.org/10.1017/CBO9780511761195.008 Published online by Cambridge University Press

Table 6.5. *Comparison of predicted non-dimensional frequencies of a simply supported square plate. HTK element*

	$\lambda^{1/2}$		
Mode	FEM [6.20]	Analytical [6.21]	% Difference
(1, 1)	0.0945	0.0930	1.61
(2, 1)	0.2347	0.2218	5.82
(2, 2)	0.3597	0.3402	5.73
(3, 1)	0.4729	0.4144	14.1
(3, 2)	0.5746	0.5197	10.6
(3, 3)	0.7520	0.6821	10.2

$\lambda = \rho h^2 \omega^2 / G$.

where $[\mathbf{I}]_3$ is defined by (6.40). These will be more accurate at a (2×2) array of integration points. The shear forces per unit length are

$$\begin{bmatrix} Q_x \\ Q_y \end{bmatrix} = \kappa h \, [\mathbf{D}^s] \, [\mathbf{B}^s] \{\mathbf{w}\}_e \tag{6.103}$$

where Q_x, Q_y act on the faces whose normals are in the x-, y-directions respectively. These will be accurate at the centre of the element.

EXAMPLE 6.7 Use the HTK element to estimate the six lowest frequencies of a moderately thick, simply supported square plate with a span/thickness ratio of 10. Take $\nu = 0.3$. Compare the results with the analytical solution given in reference [6.21].

The plate is represented by an (8×8) mesh of elements. Since the boundaries are simply supported, then w is zero at all boundary nodes. The results obtained for the non-dimensional frequency $\omega(\rho h^2/G)^{1/2}$ are compared with the analytical values in Table 6.5.

The analysis was repeated using (2×2), (4×4), (6×6) and (10×10) meshes of elements. The convergence of the lowest non-dimensional frequency with the increase in number of elements is shown in Figure 6.10.

EXAMPLE 6.8 Investigate the effect of changing the span/thickness ratio on the accuracy of the lowest frequency of a simply supported square plate. Take $\nu = 0.3$.

The plate is represented by an (8×8) mesh of elements. The lowest non-dimensional frequency $\omega(\rho h b^4/D)^{1/2}$ has been calculated for various values of the span/thickness ratio b/h. The results are shown in Figure 6.11. The analytical frequency shown is for a thin plate. As the plate gets thinner b/h increases and the non-dimensional frequency increases reaching an asymptotic value which is greater than the analytical value for a thin plate.

References [6.18, 6.19] present a number of static solutions using the HTK element. These indicate that accurate solutions can be obtained if the boundary conditions are simply supported or clamped. Reference [6.22] indicates that in the case of a cantilever plate large errors can occur.

https://doi.org/10.1017/CBO9780511761195.008 Published online by Cambridge University Press

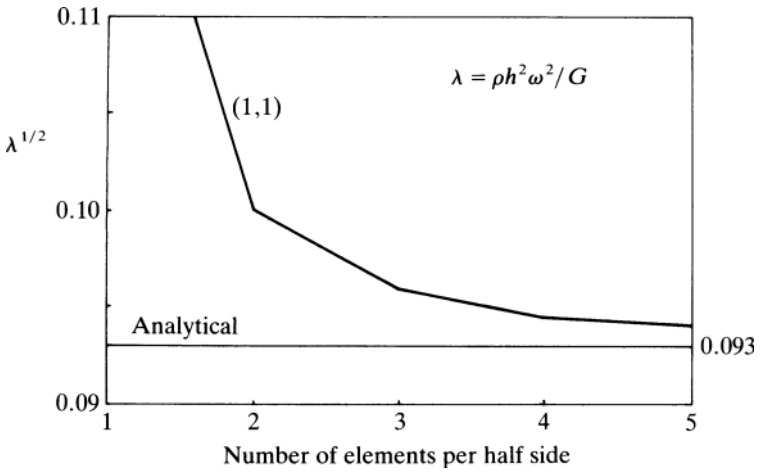

Figure 6.10. Convergence of the lowest non-dimensional frequency of a simply supported square plate. $b/h = 10$ [6.20].

6.4 Thin Triangular Element (non-conforming)

Figure 6.12 shows a triangular element with three node points, one at each vertex. There are three degrees of freedom at each node, namely, the component of displacement normal to the plane of the plate, w, and the two rotations $\theta_x = \partial w/\partial y$ and $\theta_y = -\partial w/\partial x$.

Since the element has nine degrees of freedom the displacement function can be represented by a polynomial having nine terms. A complete cubic has ten terms (see Figure 4.1). Equation (6.5) indicates that the constant, linear and quadratic terms should be retained. In order to maintain symmetry of the cubic terms the coefficients of x^2y and xy^2 are taken to be equal. Therefore

$$w = \alpha_1 + \alpha_2 x + \alpha_3 y + \alpha_4 x^2 + \alpha_5 xy + \alpha_6 y^2 + \alpha_7 x^3 + \alpha_8 (x^2 y + xy^2) + \alpha_9 y^3 \tag{6.104}$$

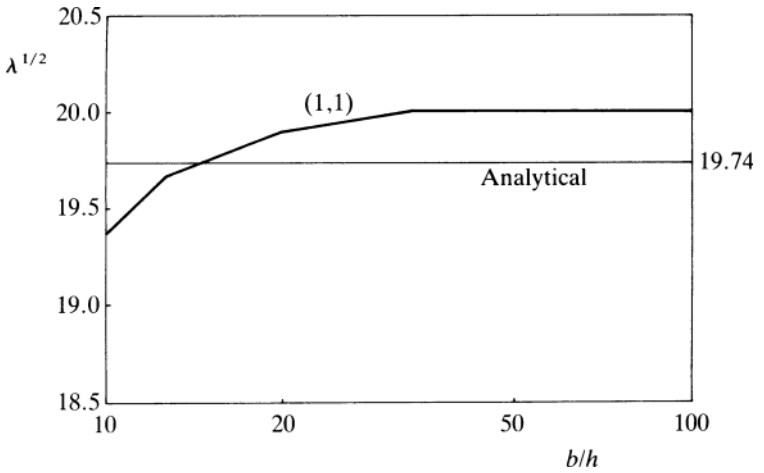

Figure 6.11. Effect of span/thickness ratio on lowest frequency of simply supported square plate [6.20].

https://doi.org/10.1017/CBO9780511761195.008 Published online by Cambridge University Press

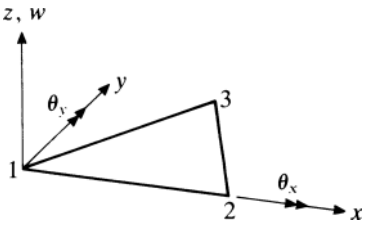

Figure 6.12. Geometry of a triangular element.

This expression can be written in the following matrix form

$$\begin{aligned} w &= \lfloor 1 \quad x \quad y \quad x^2 \quad xy \quad y^2 \quad x^3 \quad (x^2y + xy^2) \quad y^3 \rfloor \{\boldsymbol{\alpha}\} \\ &= \lfloor \mathbf{P}(x, y) \rfloor \{\boldsymbol{\alpha}\} \end{aligned} \tag{6.105}$$

where

$$\{\boldsymbol{\alpha}\}^{\mathrm{T}} = \lfloor \alpha_1 \quad \alpha_2 \quad \cdots \quad \alpha_9 \rfloor \tag{6.106}$$

Differentiating (6.105) with respect to x and y gives

$$\begin{bmatrix} w \\ \theta_x \\ \theta_y \end{bmatrix} = \begin{bmatrix} 1 & x & y & x^2 & xy & y^2 & x^3 & (x^2y + xy^2) & y^3 \\ 0 & 0 & 1 & 0 & x & 2y & 0 & (x^2 + 2xy) & 3y^2 \\ 0 & -1 & 0 & -2x & -y & 0 & -3x^2 & -(2xy + y^2) & 0 \end{bmatrix} \{\boldsymbol{\alpha}\} \tag{6.107}$$

Evaluating (6.107) at nodes 1, 2 and 3 with coordinates $(0, 0)$, $(x_2, 0)$ and (x_3, y_3) gives

$$\{\mathbf{w}\}_e = [\mathbf{A}]_e \{\boldsymbol{\alpha}\} \tag{6.108}$$

where

$$\{\mathbf{w}\}_e^{\mathrm{T}} = \lfloor w_1 \quad \theta_{x1} \quad \theta_{y1} \quad w_2 \quad \theta_{x2} \quad \theta_{y2} \quad w_3 \quad \theta_{x3} \quad \theta_{y3} \rfloor \tag{6.109}$$

and

$$[\mathbf{A}]_e = \begin{bmatrix} 1 & 0 & 0 & 0 & 0 & 0 & 0 & 0 & 0 \\ 0 & 0 & 1 & 0 & 0 & 0 & 0 & 0 & 0 \\ 0 & -1 & 0 & 0 & 0 & 0 & 0 & 0 & 0 \\ 1 & x_2 & 0 & x_2^2 & 0 & 0 & x_2^3 & 0 & 0 \\ 0 & 0 & 1 & 0 & x_2 & 0 & 0 & x_2^2 & 0 \\ 0 & -1 & 0 & -2x_2 & 0 & 0 & -3x_2^2 & 0 & 0 \\ 1 & x_3 & y_3 & x_3^2 & x_3y_3 & y_3^2 & x_3^3 & (x_3^2y_3 + x_3y_3^2) & y_3^3 \\ 0 & 0 & 1 & 0 & x_3 & 2y_3 & 0 & (x_3^2 + 2x_3y_3) & 3y_3^2 \\ 0 & -1 & 0 & -2x_3 & -y_3 & 0 & -3x_3^2 & -(2x_3y_3 + y_3^2) & 0 \end{bmatrix} \tag{6.110}$$

https://doi.org/10.1017/CBO9780511761195.008 Published online by Cambridge University Press

Solving (6.108) for $\{\boldsymbol{\alpha}\}$ gives

$$\{\boldsymbol{\alpha}\} = [\mathbf{A}]_e^{-1} \{\mathbf{w}\}_e \tag{6.111}$$

Substituting (6.111) into (6.105) gives

$$w = \lfloor \mathbf{P}(x, y) \rfloor [\mathbf{A}]_e^{-1} \{\mathbf{w}\}_e \tag{6.112}$$

Unfortunately the matrix $[\mathbf{A}]_e$ is singular whenever

$$x_2 - 2x_3 - y_3 = 0 \tag{6.113}$$

and, therefore, cannot be inverted. If this occurs the positions of the nodes should be altered to avoid this condition. This element is commonly referred to as element T [6.23].

Evaluating (6.107) along $y = 0$ gives

$$\begin{bmatrix} w \\ \theta_x \\ \theta_y \end{bmatrix} = \begin{bmatrix} 1 & x & 0 & x^2 & 0 & 0 & x^3 & 0 & 0 \\ 0 & 0 & 1 & 0 & x & 0 & 0 & x^2 & 0 \\ 0 & -1 & 0 & -2x & 0 & 0 & -3x^2 & 0 & 0 \end{bmatrix} \{\boldsymbol{\alpha}\} \tag{6.114}$$

From this it can be seen that w varies cubically and θ_y quadratically. The coefficients $\alpha_1, \alpha_2, \alpha_4$ and α_7 can be expressed in terms of w_1, θ_{y1}, w_2 and θ_{y2}, by evaluating these expressions at nodes 1 and 2. This means that the displacement and tangential slope will be continuous between elements.

On the other hand, θ_x is a quadratic function having coefficients α_3, α_5 and α_8. These cannot be determined using only the values of θ_x at nodes 1 and 2 only. Therefore, the normal slope will not be continuous between elements, and the element is a non-conforming one. The other disadvantage of this element is that the assumed function (6.104) is not invariant with respect to the choice of coordinate axes due to combining the x^2y and xy^2 terms.

Substituting (6.112) into (6.1) gives

$$T_e = \tfrac{1}{2} \{\dot{\mathbf{w}}\}_e^{\mathrm{T}} [\bar{\mathbf{m}}]_e \{\dot{\mathbf{w}}\}_e \tag{6.115}$$

where

$$[\bar{\mathbf{m}}]_e = [\mathbf{A}]_e^{-\mathrm{T}} \int_A \rho h \lfloor \mathbf{P} \rfloor^{\mathrm{T}} \lfloor \mathbf{P} \rfloor \, \mathrm{d}A \, [\mathbf{A}]_e^{-1} \tag{6.116}$$

is the element inertia matrix. A typical element in the integrand is of the form $\rho h \int_A x^m y^n \, \mathrm{d}A$. Integrals of this form can be evaluated using one of the following [6.24]

For $x_3 \neq 0, x_3 \neq x_2$:

$$\int_A x^m y^n \, \mathrm{d}A = \sum_{r=0}^{m+1} \sum_{s=0}^{r} \frac{(-1)^{r+s} m!}{(m+1-r)!(r-s)!s!(n+r+1)} x_2^{m+1-s} x_3^s y_3^{n+1} - \frac{x_3^{m+1} y_3^{n+1}}{(m+1)(m+n+2)} \tag{6.117}$$

https://doi.org/10.1017/CBO9780511761195.008 Published online by Cambridge University Press

For $x_3 = 0$:

$$\int_A x^m y^n \, \mathrm{d}A = \sum_{r=0}^{m+1} \frac{(-1)^r m!}{(m+1-r)!r!(n+r+1)} x_2^{m+1} y_3^{n+1} \tag{6.118}$$

For $x_3 = x_2$:

$$\int_A x^m y^n \, \mathrm{d}A = \frac{1}{(n+1)(m+n+2)} x_2^{m+1} y_3^{n+1} \tag{6.119}$$

Substituting (6.112) into (6.3) and (6.2) gives

$$U_e = \tfrac{1}{2}\{\mathbf{w}\}_e^{\mathrm{T}} [\bar{\mathbf{k}}]_e \{\mathbf{w}\}_e \tag{6.120}$$

where

$$[\bar{\mathbf{k}}]_e = [\mathbf{A}]_e^{-\mathrm{T}} \int_A \frac{h^3}{12} [\bar{\mathbf{B}}]^{\mathrm{T}} [\mathbf{D}] [\bar{\mathbf{B}}] \, \mathrm{d}A \, [\mathbf{A}]_e^{-1} \tag{6.121}$$

where

$$\left[\bar{\mathbf{B}}\right] = \begin{bmatrix} 0 & 0 & 0 & 2 & 0 & 0 & 6x & 2y & 0 \\ 0 & 0 & 0 & 0 & 0 & 2 & 0 & 2x & 6y \\ 0 & 0 & 0 & 0 & 2 & 0 & 0 & 4(x+y) & 0 \end{bmatrix} \tag{6.122}$$

The integrand in (6.121) can also be evaluated using (6.117)–(6.119).

Substituting (6.112) into (6.4) gives

$$\delta W_e = \{\delta \mathbf{w}\}_e^{\mathrm{T}} \{\bar{\mathbf{f}}\}_e \tag{6.123}$$

where

$$\{\bar{\mathbf{f}}\}_e = [\mathbf{A}]_e^{-\mathrm{T}} \int_A \lfloor \mathbf{P} \rfloor^{\mathrm{T}} p_z \, \mathrm{d}A \tag{6.124}$$

Again (6.117)–(6.119) should be used to evaluate the integrand.

The next step is to transform the energy expressions (6.115), (6.120) and (6.123) into expressions involving nodal degrees of freedom relative to global axes (see Figure 6.13), w, θ_X and θ_Y. The relationship between displacement components in

https://doi.org/10.1017/CBO9780511761195.008 Published online by Cambridge University Press

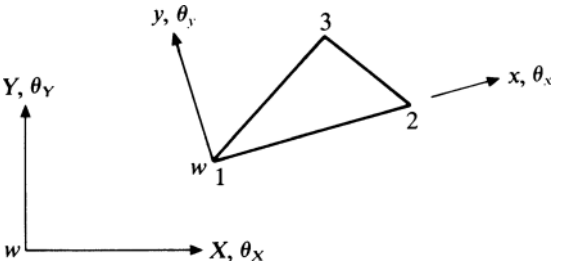

Figure 6.13. Orientation of a triangular element with respect to global axes.

local and global axes is (see Section (3.6))

$$\begin{bmatrix} w \\ \theta_x \\ \theta_y \end{bmatrix} = \begin{bmatrix} 1 & 0 & 0 \\ 0 & \cos(x, X) & \cos(x, Y) \\ 0 & \cos(y, X) & \cos(y, Y) \end{bmatrix} \begin{bmatrix} w \\ \theta_X \\ \theta_Y \end{bmatrix}$$

$$= [\mathbf{L}_2] \begin{bmatrix} w \\ \theta_X \\ \theta_Y \end{bmatrix} \tag{6.125}$$

Since the local x-axis lies along the side 1–2 and the local y-axis is perpendicular to it

$$\begin{aligned} \cos(x, X) &= X_{21}/L_{12}, \qquad \cos(x, Y) = Y_{21}/L_{12} \\ \cos(y, X) &= -Y_{21}/L_{12}, \qquad \cos(y, Y) = X_{21}/L_{12} \end{aligned} \tag{6.126}$$

where

$$X_{21} = X_2 - X_1, \qquad Y_{21} = Y_2 - Y_1 \tag{6.127}$$

and

$$L_{12} = \left(X_{21}^2 + Y_{21}^2\right)^{1/2} \tag{6.128}$$

(X_1, Y_1) and (X_2, Y_2) are the global coordinates of nodes 1 and 2.

The degrees of freedom at all three nodes of the element can be transformed from local to global axes by means of the relation

$$\{\mathbf{w}\}_e = [\mathbf{R}]_e \{\mathbf{w}\}_e \tag{6.129}$$

where

$$\{\mathbf{w}\}_e^{\mathrm{T}} = \lfloor w_1 \quad \theta_{X1} \quad \theta_{Y1} \quad w_2 \quad \theta_{X2} \quad \theta_{Y2} \quad w_3 \quad \theta_{X3} \quad \theta_{Y3} \rfloor \tag{6.130}$$

and

$$[\mathbf{R}]_e = \begin{bmatrix} \mathbf{L}_2 & \mathbf{0} & \mathbf{0} \\ \mathbf{0} & \mathbf{L}_2 & \mathbf{0} \\ \mathbf{0} & \mathbf{0} & \mathbf{L}_2 \end{bmatrix} \tag{6.131}$$

https://doi.org/10.1017/CBO9780511761195.008 Published online by Cambridge University Press

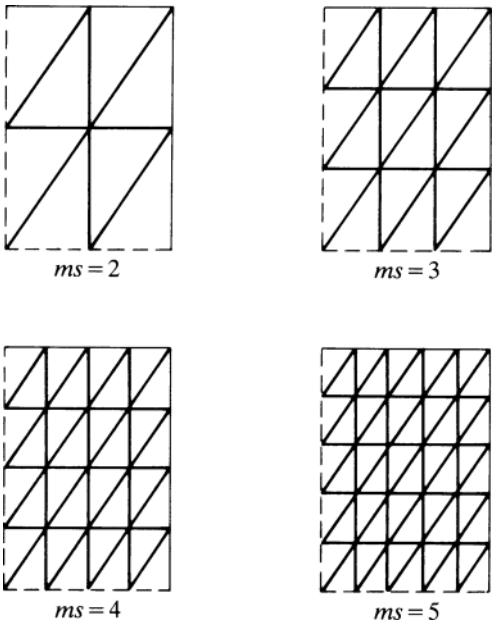

Figure 6.14. Idealisations of one quarter of a rectangular plate of aspect ratio 1.48:1. ms = mesh size.

Substituting (6.129) into (6.115), (6.120) and (6.123) gives

$$\begin{aligned} T_e &= \tfrac{1}{2}\{\dot{\mathbf{W}}\}_e^{\mathrm{T}}[\mathbf{m}]_e\{\dot{\mathbf{W}}\}_e \\ U_e &= \tfrac{1}{2}\{\mathbf{w}\}_e^{\mathrm{T}}[\mathbf{k}]_e\{\mathbf{w}\}_e \\ \delta W &= \{\delta W\}_e^{\mathrm{T}}\{\mathbf{f}\}_e \end{aligned} \tag{6.132}$$

where

$$\begin{aligned} [\mathbf{m}]_e &= [\mathbf{R}]_e^{\mathrm{T}}[\bar{\mathbf{m}}]_e[\mathbf{R}]_e \\ [\mathbf{k}]_e &= [\mathbf{R}]_e^{\mathrm{T}}[\bar{\mathbf{k}}]_e[\mathbf{R}]_e \\ \{\mathbf{f}\}_e &= [\mathbf{R}]_e^{\mathrm{T}}\{\bar{\mathbf{f}}\}_e \end{aligned} \tag{6.133}$$

When forming the element matrices referred to local axes the local coordinates of nodes 2 and 3 are required. These can be obtained from their global coordinates by means of the relation

$$\begin{bmatrix} x \\ y \end{bmatrix} = \begin{bmatrix} \cos(x, X) & \cos(x, Y) \\ \cos(y, X) & \cos(y, Y) \end{bmatrix} \begin{bmatrix} X - X_1 \\ Y - Y_1 \end{bmatrix} \tag{6.134}$$

EXAMPLE 6.9 Use the triangular element T to estimate the five lowest frequencies of a thin rectangular plate of aspect ratio 1.48:1 which is simply supported on all four edges. Compare the results with the analytical solution $\pi^2\{m^2 + (na/b)^2\}(D/\rho ha^4)^{1/2}$ rad/s, where a, b are the lengths of the sides.

One quarter of the plate was idealised in the ways indicated in Figure 6.14. The local axes were taken as indicated in Figure 6.15(a). Simply supported boundary conditions are applied along the outer boundaries and either symmetric or antisymmetric boundary conditions applied along the two axes of

https://doi.org/10.1017/CBO9780511761195.008 Published online by Cambridge University Press

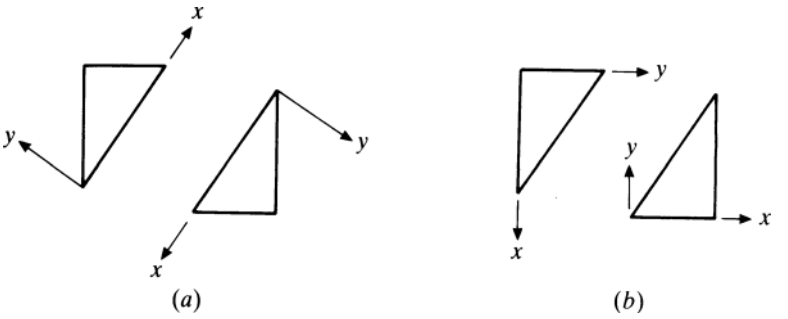

Figure 6.15. Choice of local axes for triangular elements.

symmetry. The results obtained are compared with the analytical frequencies in Figure 6.16. The frequencies obtained using the finite element method are all less than the analytical frequencies. All five modes converge monotonically for mesh sizes greater than three.

To illustrate the fact that the assumed function is not invariant with respect to the choice of local axes, the plate was analysed using a mesh size of five and the local axes as indicated in Figure 6.15(*b*). The percentage difference in frequencies when compared with the analytical solution is given for the two choices of axes shown in Figure 6.15 in Table 6.6. This indicates that quite different results are obtained depending upon the choice of local axes.

EXAMPLE 6.10 Figure 6.17 shows a triangular cantilever plate having a thickness of 1.55 mm. Use the triangular element T to calculate the six lowest frequencies and modes. Take $E = 200 \times 10^9$ N/m^2, $\nu = 0.3$ and $\rho = 7870$ kg/m^3. Compare these frequencies and mode shapes with the experimental measurements given in reference [6.26].

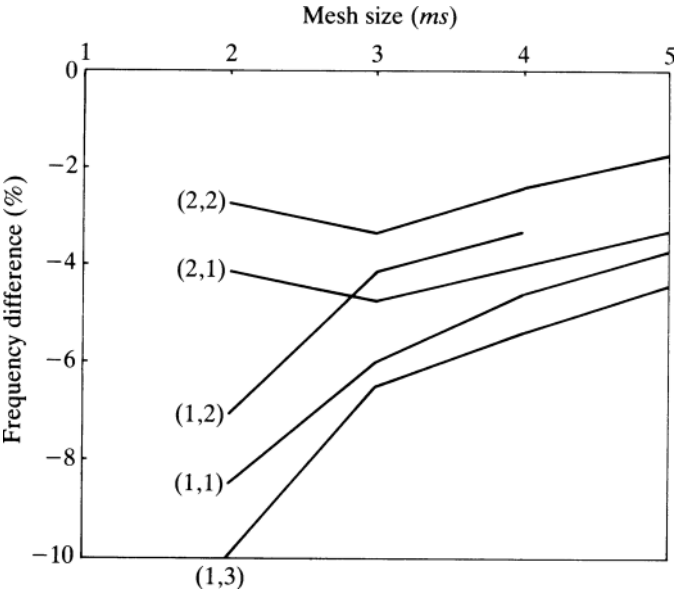

Figure 6.16. Flexural vibrations of a simply supported rectangular plate: aspect ratio 1.48:1. Element T [6.24, 6.25].

https://doi.org/10.1017/CBO9780511761195.008 Published online by Cambridge University Press

Table 6.6. *Comparison of predicted frequencies for different local axis systems of a simply supported rectangular plate: aspect ratio 1.48:1. Mesh size 5 [6.24]. Element T*

	Local axes	
Mode	6.15(*a*)	6.15(*b*)
(1, 1)	−3.77	−15.22
(2, 1)	−3.31	−12.35
(1, 3)	−4.42	−9.15
(2, 2)	−1.74	+6.05

Two idealisations were used in analysing the plate as shown in Figures 6.18(*a*) and (*b*). The mesh sizes 5 and 10 consisted of 25 and 100 elements respectively. The local axes used are the ones illustrated in Figure 6.15(*a*).

The percentage differences between the predicted and measured frequencies are given in Table 6.7. For a mesh size of 5 these values vary from −2.43 to +18.98. Increasing the mesh size to 10 reduces this range to (−3.26, +0.79). A comparison of the predicted and measured modal patterns is given in Figure 6.19. The first mode is the fundamental bending mode.

6.5 Thin Triangular Element (conforming)

One way of achieving continuity of the lateral displacement and both its first derivatives between elements, is to ensure that the normal slope varies linearly along an edge, as indicated in Section 6.1. This technique is used in reference [6.27] to derive a conforming thin triangular element (HCT) in Cartesian coordinates. The element has also been derived using area coordinates in reference [6.28] (where it is called LCCT-9). Both derivations are presented for comparison.

6.5.1 Cartesian Coordinates

Figure 6.20(*a*) shows a triangular element divided into three sub-triangles. The interior point 0 may be located arbitrarily, but it is convenient to position it at the centroid of the triangle. X, Y are the global axes of the system. It is convenient to use local axes x, y for each sub-triangle, where x is parallel to the exterior edge of the sub-triangle and y is perpendicular to it. Both the local and global axes for sub-triangle 1 are indicated in Figure 6.20(*b*).

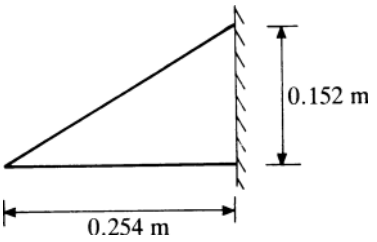

Figure 6.17. Geometry of a triangular cantilever plate.

https://doi.org/10.1017/CBO9780511761195.008 Published online by Cambridge University Press

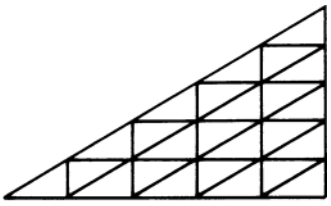

(*a*) Mesh size 5

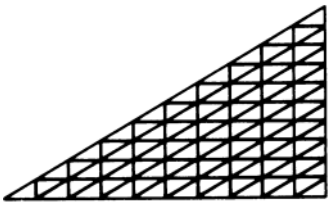

(*b*) Mesh size 10

Figure 6.18. Idealisation of a triangular plate using triangular elements.

Independent displacement functions are used for each sub-triangle. For example, for sub-triangle 1 it is assumed that

$$w^{(1)} = \lfloor \mathbf{P}^{(1)} \rfloor \{\boldsymbol{\alpha}^{(1)}\} \tag{6.135}$$

where

$$\lfloor \mathbf{P}^{(1)} \rfloor = \lfloor 1 \quad x \quad y \quad x^2 \quad xy \quad y^2 \quad x^3 \quad xy^2 \quad y^3 \rfloor \tag{6.136}$$

Note that the term x^2y has been omitted to ensure that $\partial w/\partial y$ varies linearly with x along the side 2–3.

Substituting (6.135) into (6.1) gives

$$T_e^{(1)} = \tfrac{1}{2}\{\dot{\boldsymbol{\alpha}}^{(1)}\}^{\mathrm{T}}[\bar{\mathbf{m}}^{(1)}]\{\dot{\boldsymbol{\alpha}}^{(1)}\} \tag{6.137}$$

where

$$[\bar{\mathbf{m}}^{(1)}] = \int_{A_1} \rho h \lfloor \mathbf{P}^{(1)} \rfloor^{\mathrm{T}} [\mathbf{P}^{(1)}] \, \mathrm{d}A \tag{6.138}$$

Table 6.7. *Comparison of predicted and measured frequencies of a triangular cantilever plate. Element T*

Mode number	Measured frequency (Hz) [6.26]	Predicted frequencies (% difference) [6.24]	
		$ms = 5$	$ms = 10$
1	37.5	−2.43	−2.88
2	161.0	−0.82	−3.26
3	243.0	+8.65	+0.75
4	392.0	+9.43	−1.48
5	592.0	+5.76	−0.76
6	744.0	+18.98	+0.79

https://doi.org/10.1017/CBO9780511761195.008 Published online by Cambridge University Press

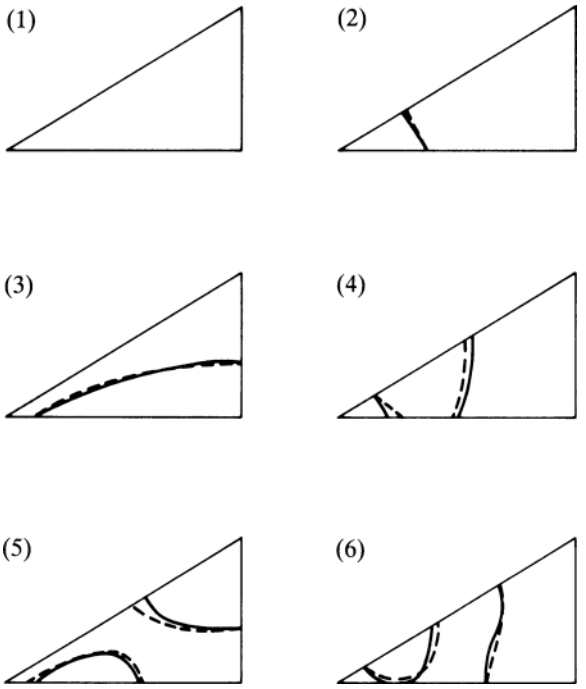

Figure 6.19. Comparison of predicted and measured modal patterns of a triangular cantilever plate [6.24]. —— Measured, – – – predicted.

and A_1 is the area of sub-triangle 1. This expression can be evaluated using the technique described in Section 6.4. This procedure is repeated for each of the three sub-triangles. Adding the kinetic energies together gives

$$T_e = \tfrac{1}{2}\{\dot{\boldsymbol{\alpha}}\}^{\mathrm{T}}\,[\bar{\mathbf{m}}]_e\,\{\dot{\boldsymbol{\alpha}}\} \tag{6.139}$$

where

$$[\bar{\mathbf{m}}]_e = \begin{bmatrix} [\bar{\mathbf{m}}^{(1)}] & & \\ & [\bar{\mathbf{m}}^{(2)}] & \\ & & [\bar{\mathbf{m}}^{(3)}] \end{bmatrix}, \qquad \{\boldsymbol{\alpha}\} = \begin{bmatrix} \{\boldsymbol{\alpha}^{(1)}\} \\ \{\boldsymbol{\alpha}^{(2)}\} \\ \{\boldsymbol{\alpha}^{(3)}\} \end{bmatrix} \tag{6.140}$$

The column matrix $\{\boldsymbol{\alpha}\}$ consists of 27 coefficients. Eighteen constraints are applied to ensure internal compatibility between the sub-triangles. This reduces the

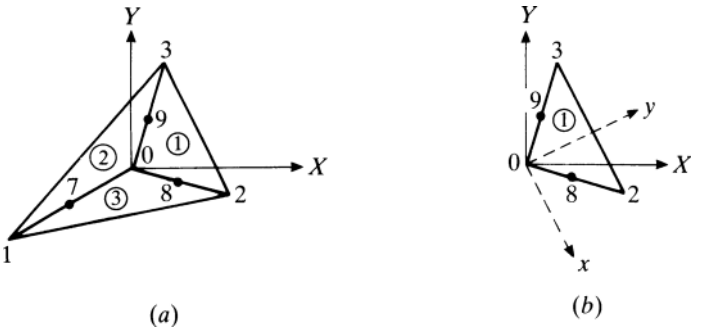

Figure 6.20. Geometry of a triangular element divided into three sub-triangles.

https://doi.org/10.1017/CBO9780511761195.008 Published online by Cambridge University Press

number of unknown coefficients to nine which are expressed in terms of the three degrees of freedom w, θ_X, θ_Y at the three nodes 1, 2 and 3.

The displacement and rotations with respect to local axes for sub-triangle 1 are

$$\begin{bmatrix} w \\ \theta_x \\ \theta y \end{bmatrix} = \begin{bmatrix} 1 & x & y & x^2 & xy & y^2 & x^3 & xy^2 & y^3 \\ 0 & 0 & 1 & 0 & x & 2y & 0 & 2xy & 3y^2 \\ 0 & -1 & 0 & -2x & -y & 0 & -3x^2 & -y^2 & 0 \end{bmatrix} \{\boldsymbol{\alpha}^{(1)}\} \quad (6.141)$$

Evaluating (6.141) at node 2 gives

$$\begin{bmatrix} w \\ \theta_x \\ \theta_y \end{bmatrix}_2 = \{\bar{\mathbf{w}}^{(1)}\}_2 = [\bar{\mathbf{A}}^{(1)}]_2 \{\boldsymbol{\alpha}^{(1)}\} \quad (6.142)$$

where

$$[\bar{\mathbf{A}}^{(1)}]_2 = \begin{bmatrix} 1 & x_2 & y_2 & x_2^2 & x_2 y_2 & y_2^2 & x_2^3 & x_2 y_2^2 & y_2^3 \\ 0 & 0 & 1 & 0 & x_2 & 2y_2 & 0 & 2x_2 y_2 & 3y_2^2 \\ 0 & -1 & 0 & -2x_2 & -y_2 & 0 & -3x_2^2 & -y_2^2 & 0 \end{bmatrix} \quad (6.143)$$

and (x_2, y_2) are the local coordinates of node 2. These can be calculated from the global coordinates by the procedure described in the previous section.

Transforming (6.142) to global axes gives

$$\begin{aligned} \begin{bmatrix} w \\ \theta_X \\ \theta_Y \end{bmatrix}_2 &= \{\mathbf{w}^{(1)}\}_2 = [\mathbf{L}_2^{(1)}]^{\mathrm{T}} \{\bar{\mathbf{w}}^{(1)}\}_2 \\ &= [\mathbf{L}_2^{(1)}]^{\mathrm{T}} [\bar{\mathbf{A}}^{(1)}]_2 \{\boldsymbol{\alpha}^{(1)}\} = [\mathbf{A}^{(1)}]_2 \{\boldsymbol{\alpha}^{(1)}\} \end{aligned} \quad (6.144)$$

where $[\mathbf{L}_2^{(1)}]$ is of the form (6.125). Similar expressions may be written for the other nodes in this and the other two sub-triangles.

Compatibility of displacement and tangential slope is achieved by equating the degrees of freedom at common nodes of the three sub-triangles. This gives

$$\begin{aligned} \{\mathbf{w}^{(3)}\}_1 &= \{\mathbf{w}^{(2)}\}_1 \\ \{\mathbf{w}^{(1)}\}_2 &= \{\mathbf{w}^{(3)}\}_2 \\ \{\mathbf{w}^{(2)}\}_3 &= \{\mathbf{w}^{(1)}\}_3 \\ \{\mathbf{w}^{(2)}\}_0 &= \{\mathbf{w}^{(3)}\}_0 \\ \{\mathbf{w}^{(1)}\}_0 &= \{\mathbf{w}^{(2)}\}_0 \end{aligned} \quad (6.145)$$

https://doi.org/10.1017/CBO9780511761195.008 Published online by Cambridge University Press

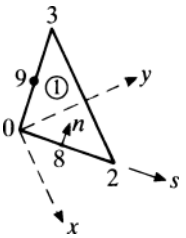

Figure 6.21. Geometry of a sub-triangle.

Compatibility of normal slope along the interior edges of the sub-triangles is ensured by equating the normal slopes at their mid-points 7, 8 and 9. The method of calculating the normal slope will be illustrated by considering the point 8 of sub-triangle 1 (see Figure 6.21). If s is the direction from 0 to the exterior node 2 and n is normal to this, then

$$\begin{aligned}\left(\frac{\partial w^{(1)}}{\partial n}\right)_8 &= \lfloor 0 \quad \cos(s,x) \quad \cos(s,y)\rfloor_8 \{\bar{\mathbf{w}}^{(1)}\}_8 \\ &= \lfloor 0 \quad \cos(s,x) \quad \cos(s,y)\rfloor_5 [\bar{\mathbf{A}}^{(1)}]_8 \{\boldsymbol{\alpha}^{(1)}\} \\ &= \lfloor \mathbf{A}^{(1)} \rfloor_8 \{\boldsymbol{\alpha}^{(1)}\}\end{aligned} \tag{6.146}$$

Similarly for the other interior node of sub-triangle 1 and the other sub-triangles. The three conditions imposing compatibility of normal slopes between the sub-triangles are

$$\begin{aligned}\left(\frac{\partial w^{(3)}}{\partial n}\right)_7 &= \left(\frac{\partial w^{(2)}}{\partial n}\right)_7 \\ \left(\frac{\partial w^{(1)}}{\partial n}\right)_8 &= \left(\frac{\partial w^{(3)}}{\partial n}\right)_8 \\ \left(\frac{\partial w^{(2)}}{\partial n}\right)_9 &= \left(\frac{\partial w^{(1)}}{\partial n}\right)_9\end{aligned} \tag{6.147}$$

The relationships (6.145) and (6.147) are the eighteen constraints required to ensure internal compatibility. The remaining nine coefficients in (6.140) are obtained by relating the sub-triangle degrees of freedom at the external nodes to the degrees of freedom of the complete triangle, that is

$$\begin{aligned}\{\mathbf{w}\}_1 &= \{\mathbf{w}^{(3)}\}_1 \\ \{\mathbf{w}\}_2 &= \{\mathbf{w}^{(1)}\}_2 \\ \{\mathbf{w}\}_3 &= \{\mathbf{w}^{(2)}\}_3\end{aligned} \tag{6.148}$$

https://doi.org/10.1017/CBO9780511761195.008 Published online by Cambridge University Press

Substituting (6.144) into (6.145), (6.146) into (6.147) and combining with (6.148) gives

$$\begin{bmatrix} \{\mathbf{w}\}_1 \\ \{\mathbf{w}\}_2 \\ \{\mathbf{w}\}_3 \\ 0 \\ 0 \\ 0 \\ 0 \\ 0 \\ 0 \\ 0 \\ 0 \\ 0 \end{bmatrix} = \begin{bmatrix} 0 & 0 & [\mathbf{A}^{(3)}]_1 \\ [\mathbf{A}^{(1)}]_2 & 0 & 0 \\ 0 & [\mathbf{A}^{(2)}]_3 & 0 \\ 0 & -[\mathbf{A}^{(2)}]_1 & [\mathbf{A}^{(3)}]_1 \\ [\mathbf{A}^{(1)}]_2 & 0 & -[\mathbf{A}^{(3)}]_2 \\ -[\mathbf{A}^{(1)}]_3 & [\mathbf{A}^{(2)}]_3 & 0 \\ 0 & [\mathbf{A}^{(2)}]_0 & -[\mathbf{A}^{(3)}]_0 \\ [\mathbf{A}^{(1)}]_0 & -[\mathbf{A}^{(2)}]_0 & 0 \\ 0 & -[\mathbf{A}^{(2)}]_7 & [\mathbf{A}^{(3)}]_7 \\ [\mathbf{A}^{(1)}]_8 & 0 & -[\mathbf{A}^{(3)}]_8 \\ -[\mathbf{A}^{(1)}]_9 & [\mathbf{A}^{(2)}]_9 & 0 \end{bmatrix} \begin{bmatrix} \{\boldsymbol{\alpha}^{(1)}\} \\ \{\boldsymbol{\alpha}^{(2)}\} \\ \{\boldsymbol{\alpha}^{(3)}\} \end{bmatrix} \tag{6.149}$$

This equation may be written symbolically as

$$\begin{bmatrix} \{\mathbf{w}\}_e \\ 0 \end{bmatrix} = \begin{bmatrix} [\mathbf{A}_{11}] & [\mathbf{A}_{10}] \\ [\mathbf{A}_{01}] & [\mathbf{A}_{00}] \end{bmatrix} \begin{bmatrix} \{\boldsymbol{\alpha}^{(1)}\} \\ \{\boldsymbol{\alpha}^{(0)}\} \end{bmatrix} \tag{6.150}$$

Solving for $\{\boldsymbol{\alpha}^{(0)}\}$ from the second of these two matrix equations gives

$$\{\boldsymbol{\alpha}^{(0)}\} = -[\mathbf{A}_{00}]^{-1}[\mathbf{A}_{01}]\{\boldsymbol{\alpha}^{(1)}\} \tag{6.151}$$

Substituting into the first equation in (6.150) gives

$$\begin{aligned} \{\mathbf{w}\}_e &= [[\mathbf{A}_{11}] - [\mathbf{A}_{10}][\mathbf{A}_{00}]^{-1}[\mathbf{A}_{01}]]\{\boldsymbol{\alpha}^{(1)}\} \\ &= [\bar{\mathbf{A}}]\{\boldsymbol{\alpha}^{(1)}\} \end{aligned} \tag{6.152}$$

Solving for $\{\boldsymbol{\alpha}^{(1)}\}$ gives

$$\{\boldsymbol{\alpha}^{(1)}\} = [\bar{\mathbf{A}}]^{-1}\{\mathbf{w}\}_e \tag{6.153}$$

Combining (6.151) and (6.153) gives

$$\begin{aligned} \begin{bmatrix} \{\boldsymbol{\alpha}^{(1)}\} \\ \{\boldsymbol{\alpha}^{(0)}\} \end{bmatrix} &= \begin{bmatrix} [\bar{\mathbf{A}}]^{-1} \\ -[\mathbf{A}_{00}]^{-1}[\mathbf{A}_{01}][\bar{\mathbf{A}}]^{-1} \end{bmatrix} \{\mathbf{w}\}_e \\ &= \begin{bmatrix} \bar{\bar{\mathbf{A}}} \end{bmatrix} \{\mathbf{w}\}_e \end{aligned} \tag{6.154}$$

Substituting (6.154) into (6.139) gives the element inertia matrix in terms of the nine nodal degrees of freedom

$$[\mathbf{m}]_e = [\bar{\bar{\mathbf{A}}}]^{\mathrm{T}}[\bar{\mathbf{m}}]_e[\bar{\bar{\mathbf{A}}}] \tag{6.155}$$

The stiffness and equivalent nodal force matrices can be derived in a similar manner. The stiffness matrix is given by

$$[\mathbf{k}]_e = [\bar{\bar{\mathbf{A}}}]^{\mathrm{T}}[\bar{\mathbf{k}}]_e[\bar{\bar{\mathbf{A}}}] \tag{6.156}$$

https://doi.org/10.1017/CBO9780511761195.008 Published online by Cambridge University Press

where

$$[\bar{\mathbf{k}}]_e = \begin{bmatrix} [\bar{\mathbf{k}}^{(1)}] & & \\ & [\bar{\mathbf{k}}^{(2)}] & \\ & & [\bar{\mathbf{k}}^{(3)}] \end{bmatrix} \tag{6.157}$$

A typical element of this matrix is

$$[\bar{\mathbf{k}}^{(1)}] = \int_{A_1} \frac{h^3}{12} [\bar{\mathbf{B}}^{(1)}]^{\mathrm{T}} [\mathbf{D}] [\bar{\mathbf{B}}^{(1)}] \, \mathrm{d}A \tag{6.158}$$

where

$$[\bar{\mathbf{B}}^{(1)}] = \begin{bmatrix} 0 & 0 & 0 & 2 & 0 & 0 & 6x & 0 & 0 \\ 0 & 0 & 0 & 0 & 0 & 2 & 0 & 2x & 6y \\ 0 & 0 & 0 & 0 & 2 & 0 & 0 & 4y & 0 \end{bmatrix} \tag{6.159}$$

The equivalent nodal force matrix is

$$\{\mathbf{f}\}_e = [\bar{\bar{\mathbf{A}}}]^{\mathrm{T}} \{\bar{\mathbf{f}}\}_e \tag{6.160}$$

where

$$\{\bar{\mathbf{f}}\}_e = \begin{bmatrix} \{\bar{\mathbf{f}}^{(1)}\} \\ \{\bar{\mathbf{f}}^{(2)}\} \\ \{\bar{\mathbf{f}}^{(3)}\} \end{bmatrix} \tag{6.161}$$

A typical element of this matrix is

$$\{\bar{\mathbf{f}}^{(1)}\} = \int_{A_1} \lfloor \mathbf{P}^{(1)} \rfloor^{\mathrm{T}} p_z \, \mathrm{d}A \tag{6.162}$$

6.5.2 Area Coordinates

When using area coordinates the displacement function for a sub-triangle is initially assumed to be a complete cubic which has ten terms. Therefore, the matrix $\lfloor \mathbf{P}^{(1)} \rfloor$ in (6.135) is

$$[\mathbf{P}^{(1)}] = \lfloor L_1^3 \quad L_2^3 \quad L_3^3 \quad L_1^2 L_2 \quad L_1^2 L_3 \quad L_2^2 L_3 \quad L_1 L_2^2 \quad L_1 L_3^2 \quad L_2 L_3^2 \quad L_1 L_2 L_3 \rfloor \tag{6.163}$$

The inertia matrix $[\bar{\mathbf{m}}^{(1)}]$ expressed in terms of the coefficients $\{\boldsymbol{\alpha}^{(1)}\}$ (see expressions (6.137) and (6.138)) can be evaluated using (4.90). This results in the

https://doi.org/10.1017/CBO9780511761195.008 Published online by Cambridge University Press

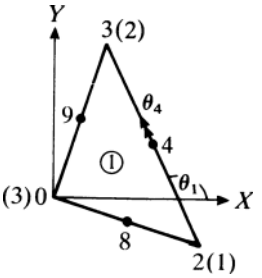

Figure 6.22. Geometry of sub-triangle 1.

following matrix.

$$\left[\bar{\mathbf{m}}^{(1)}\right] = \frac{\rho h A^{(1)}}{5040}\begin{bmatrix} 180 & & & & & & & & & \\ 9 & 180 & & & & & & & & \\ 9 & 9 & 180 & & & & & \text{Sym} & & \\ 30 & 12 & 3 & 12 & & & & & & \\ 30 & 3 & 12 & 6 & 12 & & & & & \\ 3 & 30 & 12 & 3 & 2 & 12 & & & & \\ 12 & 30 & 3 & 9 & 3 & 6 & 12 & & & \\ 12 & 3 & 30 & 3 & 9 & 3 & 2 & 12 & & \\ 3 & 12 & 30 & 2 & 3 & 9 & 3 & 6 & 12 & \\ 6 & 6 & 6 & 3 & 3 & 3 & 3 & 3 & 3 & 2 \end{bmatrix} \tag{6.164}$$

The ten coefficients in $\{\boldsymbol{\alpha}^{(1)}\}$ are expressed in terms of w, θ_X, θ_Y at nodes 0, 2 and 3 (see Figure 6.22) and the normal slope, θ_4, at node 4 which is located at the mid-point of side 2–3. The node numbers in brackets are the numbers used for the area coordinates. This calculation is carried out using the relations

$$\begin{aligned} \theta_X &= \frac{\partial w^{(1)}}{\partial Y} = \frac{1}{2A_1}\sum_{j=1}^{3} b_j \frac{\partial w^{(1)}}{\partial L_j} \\ \theta_Y &= -\frac{\partial w^{(1)}}{\partial X} = \frac{1}{2A_1}\sum_{j=1}^{3} a_j \frac{\partial w^{(1)}}{\partial L_j} \end{aligned} \tag{6.165}$$

from (4.96), where a_j and b_j are defined in (4.10) and

$$\begin{aligned} \theta_4 &= (\cos\theta_1\theta_X + \sin\theta_1\theta_Y)_4 \\ &= \left(\frac{b_3}{l_3}\theta_X - \frac{a_3}{l_3}\theta_Y\right)_4 \end{aligned} \tag{6.166}$$

where

$$l_3 = \left(a_3^2 + b_3^2\right)^{1/2} \tag{6.167}$$

The result is

$$\left\{\boldsymbol{\alpha}^{(1)}\right\} = [\bar{\mathbf{c}}]\left\{\mathbf{w}^{(1)}\right\} \tag{6.168}$$

https://doi.org/10.1017/CBO9780511761195.008 Published online by Cambridge University Press

where

$$\left\{\mathbf{w}^{(1)}\right\}^{\mathrm{T}} = \lfloor w_2 \quad \theta_{X2} \quad \theta_{Y2} \quad w_3 \quad \theta_{X3} \quad \theta_{Y3} \quad \theta_4 \quad w_0 \quad \theta_{X0} \quad \theta_{Y0} \rfloor \tag{6.169}$$

The non-zero elements of $[\bar{\mathbf{c}}]$ are

$$\begin{aligned}
\bar{c}_{11} &= \bar{c}_{24} = \bar{c}_{36} = 1 \\
\bar{c}_{41} &= \bar{c}_{51} = \bar{c}_{64} = \bar{c}_{74} = \bar{c}_{88} = \bar{c}_{98} = 3 \\
-\bar{c}_{65} &= \bar{c}_{99} = a_1 \\
\bar{c}_{52} &= -\bar{c}_{89} = a_2 \\
-\bar{c}_{42} &= \bar{c}_{75} = a_3 \\
-\bar{c}_{66} &= \bar{c}_{9,10} = b_1 \\
\bar{c}_{53} &= -\bar{c}_{8,10} = b_2 \\
-\bar{c}_{43} &= \bar{c}_{76} = b_3 \\
\bar{c}_{10,1} &= 6\mu_3 \\
\bar{c}_{10,2} &= (a_1 - a_3\mu_3) \\
\bar{c}_{10,3} &= (b_1 - b_3\mu_3) \\
\bar{c}_{10,4} &= 6\lambda_3 \\
\bar{c}_{10,5} &= (a_3\lambda_3 - a_2) \\
\bar{c}_{10,6} &= (b_3\lambda_3 - b_2) \\
\bar{c}_{10,7} &= 4h_3
\end{aligned} \tag{6.170}$$

where

$$\begin{aligned}
\lambda_3 &= -(a_2a_3 + b_2b_3)/l_3^2 \\
\mu_3 &= 1 - \lambda_3 \\
h_3 &= 2A_1/l_3 \\
A_1 &= \tfrac{1}{2}(a_1b_2 - a_2b_1)
\end{aligned} \tag{6.171}$$

Substituting (6.168) into (6.137) gives

$$T_e^{(1)} = \tfrac{1}{2}\left\{\dot{\mathbf{w}}^{(1)}\right\}^{\mathrm{T}}\left[\mathbf{m}^{(1)}\right]\left\{\dot{\mathbf{w}}^{(1)}\right\} \tag{6.172}$$

where

$$\left[\mathbf{m}^{(1)}\right] = [\bar{\mathbf{c}}]^{\mathrm{T}}\left[\bar{\mathbf{m}}^{(1)}\right][\bar{\mathbf{c}}] \tag{6.173}$$

The inertia matrices for sub-triangles 2 and 3 are obtained in a similar manner. These matrices are then assembled together to give the inertia matrix, $[\bar{\mathbf{m}}]_e$, of the

https://doi.org/10.1017/CBO9780511761195.008 Published online by Cambridge University Press

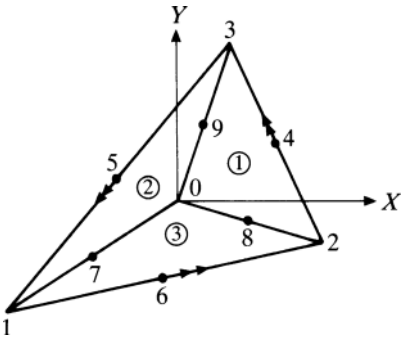

Figure 6.23. Geometry of triangular element divided into three sub-triangles.

complete triangle shown in Figure 6.23 in terms of the degrees of freedom.

$$\lfloor w_1 \quad \theta_{X1} \quad \theta_{Y1} \quad w_2 \quad \theta_{X2} \quad \theta_{Y2} \quad w_3 \quad \theta_{X3} \quad \theta_{Y3} \quad \theta_4 \quad \theta_5 \quad \theta_6 \quad w_0 \quad \theta_{X0} \quad \theta_{Y0} \rfloor = \begin{bmatrix} \{\bar{\mathbf{w}}\} \\ \{\mathbf{w}^{(0)}\} \end{bmatrix}^{\mathrm{T}} \tag{6.174}$$

In assembling these matrices it is assumed that displacement and rotations at common nodes of the three sub-triangles are equal. This will ensure compatibility of displacement and tangential slope along their common edges. Compatibility of normal slope along these same edges (0–1, 0–2 and 0–3 in Figure 6.23) is ensured by equating the normal slopes at their mid-points 7, 8 and 9. These can be obtained using relationships similar to (6.166). This will give three equations of the form

$$[\mathbf{B}_n \quad \mathbf{B}_0] \begin{bmatrix} \{\bar{\mathbf{w}}\} \\ \{\mathbf{w}^{(0)}\} \end{bmatrix} = 0 \tag{6.175}$$

which can be used to eliminate $\{\mathbf{w}^{(0)}\}$. Rearranging (6.175) gives

$$\{\mathbf{w}^{(0)}\} = -[\mathbf{B}_0]^{-1}[\mathbf{B}_n]\{\bar{\mathbf{w}}\} \tag{6.176}$$

Therefore

$$\begin{bmatrix} \{\bar{\mathbf{w}}\} \\ \{\mathbf{w}^{(0)}\} \end{bmatrix} = \begin{bmatrix} [\mathbf{I}] \\ -[\mathbf{B}_0]^{-1}[\mathbf{B}_n] \end{bmatrix} \{\bar{\mathbf{w}}\} = [\bar{\mathbf{A}}]\{\bar{\mathbf{w}}\} \tag{6.177}$$

The inertia matrix in terms of degrees of freedom at nodes 1 to 6 only is, therefore

$$[\mathbf{m}^{12}]_e = [\bar{\mathbf{A}}]^{\mathrm{T}}[\bar{\mathbf{m}}]_e[\bar{\mathbf{A}}] \tag{6.178}$$

This matrix is of order (12×12) and is referred to as the LCCT-12 element in reference [6.28]. The LCCT-9 element is obtained by constraining the normal slopes to vary linearly along each side of the complete triangle. At node 4 (see equation (6.166))

$$\begin{aligned} \theta_4 &= \frac{b_3}{l_3}\theta_{X4} - \frac{a_3}{l_3}\theta_{Y4} \\ &= \frac{b_3}{2l_3}(\theta_{X2} + \theta_{X3}) - \frac{a_3}{2l_3}(\theta_{Y2} + \theta_{Y3}) \end{aligned} \tag{6.179}$$

https://doi.org/10.1017/CBO9780511761195.008 Published online by Cambridge University Press

Similar relationships can be derived for θ_5 and θ_6. Defining

$$\{\mathbf{w}\}^{\mathrm{T}} = \lfloor w_1 \quad \theta_{X1} \quad \theta_{Y1} \quad w_2 \quad \theta_{X2} \quad \theta_{Y2} \quad w_3 \quad \theta_{X3} \quad \theta_{Y3} \rfloor \tag{6.180}$$

and

$$\{\theta\}^{\mathrm{T}} = \lfloor \theta_4 \quad \theta_5 \quad \theta_6 \rfloor \tag{6.181}$$

then these relationships can be written in the form

$$\{\boldsymbol{\theta}\} = [\mathbf{A}_c]\{\mathbf{w}\} \tag{6.182}$$

Therefore

$$\{\bar{\mathbf{w}}\} = \begin{bmatrix} \{\mathbf{w}\} \\ \{\boldsymbol{\theta}\} \end{bmatrix} = \begin{bmatrix} [\mathbf{I}] \\ [\mathbf{A}_c] \end{bmatrix} \{\mathbf{w}\} = [\bar{\bar{\mathbf{A}}}]\,\{\mathbf{w}\} \tag{6.183}$$

The inertia matrix in terms of degrees of freedom at nodes 1 to 3 is, therefore

$$[\mathbf{m}^9]_e = [\bar{\bar{\mathbf{A}}}]^{\mathrm{T}}[\mathbf{m}^{12}]_e[\bar{\bar{\mathbf{A}}}] \tag{6.184}$$

The stiffness and equivalent nodal force matrices can be derived in a similar manner. The stiffness matrix of sub-triangle 1 in terms of the coefficients $\{\boldsymbol{\alpha}^{(1)}\}$ is

$$\left[\bar{\mathbf{k}}^{(1)}\right] = \int_{A_1} \frac{h^3}{12}\left[\mathbf{B}^{(1)}\right]^{\mathrm{T}}[\mathbf{D}]\left[\mathbf{B}^{(1)}\right] \mathrm{d}A \tag{6.185}$$

The components of strain are defined as

$$\left\{\boldsymbol{\chi}^{(1)}\right\} = \begin{bmatrix} \partial^2 w^{(1)}/\partial x^2 \\ \partial^2 w^{(1)}/\partial y^2 \\ 2\partial^2 w^{(1)}/\partial x \partial y \end{bmatrix} \tag{6.186}$$

Using (4.96) to convert to derivatives with respect to area coordinates gives

$$\begin{aligned} \frac{\partial^2}{\partial x^2} &= \frac{1}{4A_1^2}\sum_{j=1}^{3}\sum_{k=1}^{3} a_j a_k \frac{\partial^2}{\partial L_j \partial L_k} \\ \frac{\partial^2}{\partial y^2} &= \frac{1}{4A_1^2}\sum_{j=1}^{3}\sum_{k=1}^{3} b_j b_k \frac{\partial^2}{\partial L_j \partial L_k} \\ \frac{\partial^2}{\partial x \partial y} &= \frac{1}{4A_1^2}\sum_{j=1}^{3}\sum_{k=1}^{3} a_j b_k \frac{\partial^2}{\partial L_j \partial L_k} \end{aligned} \tag{6.187}$$

Since $\lfloor \mathbf{P}^{(1)} \rfloor$ is cubic, the strain matrix will be linear. It can, therefore, be written in the form

$$\left[\mathbf{B}^{(1)}\right] = \frac{1}{4A_1^2}[L_1[\mathbf{W}_1] + L_2[\mathbf{W}_2] + L_3[\mathbf{W}_3]] \tag{6.188}$$

where $[\mathbf{W}_1]$, $[\mathbf{W}_2]$ and $[\mathbf{W}_3]$ are each (3×10) matrices of constants. This form will facilitate the evaluation of (6.185).

https://doi.org/10.1017/CBO9780511761195.008 Published online by Cambridge University Press

Table 6.8. *Percentage difference between finite element and analytical frequencies of a simply supported plate of aspect ratio 1.48:1*

Mesh size	2		3		4	
Mode	(1, 1)	(1, 3)	(1, 1)	(1, 3)	(1, 1)	(1, 3)
T [6.24]	−8.5	−10.0	−6.1	−6.6	−4.7	−5.4
HCT [6.29]	4.7	16.1	1.9	6.6	1.1	3.5

The equivalent force matrix in terms of the parameters $\{\boldsymbol{\alpha}^{(1)}\}$ is

$$\{\bar{\mathbf{f}}^{(1)}\} = \int_{A_1} \lfloor \mathbf{P}^{(1)} \rfloor^{\mathrm{T}} p_z \, \mathrm{d}A \tag{6.189}$$

EXAMPLE 6.11 Use the triangular elements T and HCT to estimate the two lowest frequencies of doubly symmetric modes of a thin rectangular plate of aspect ratio 1.48:1 which is simply supported on all four edges. Compare the results with the analytical solution $\pi^2[m^2 + (na/b)^2](D/\rho h a^4)^{1/2}$ rad/s where a, b are the lengths of the sides.

The plate was analysed using mesh sizes 2, 3 and 4 indicated in Figure 6.14. In the case of element T the local axes used are the ones shown in Figure 6.15(a). The frequencies predicted using the finite element method are compared with the analytical frequencies in Table 6.8. Element T underestimates the frequencies of these two modes whilst element HCT overestimates them. The HCT element results are seen to converge faster than those obtained with the element T.

EXAMPLE 6.12 Use the triangular elements LCCT-9 and LCCT-12 to estimate the two lowest frequencies of doubly symmetric modes of a thin square plate which is simply supported on all four edges. Compare the results with the analytical solution given in Example 6.1.

The plate was analysed using mesh sizes 2, 3 and 4 indicated in Figure 6.14. The frequencies are compared in Table 6.9. Both elements give results which converge from above, but the results for the LCCT-12 element are considerably more accurate than the LCCT-9 results. Reference [6.33] quotes results obtained using the HCT element which agree with those quoted in Table 6.9 for the LCCT-9 element confirming that the two elements are equivalent.

Table 6.9. *Percentage difference between finite element and analytical frequencies of a simply supported square plate*

Mesh size	2		3		4	
Mode	(1, 1)	(1, 3)	(1, 1)	(1, 3)	(1, 1)	(1, 3)
LCCT-9	2.84	15.5	1.24	5.95	0.69	3.12
LCCT-12	0.20	1.70	0.06	0.55	0.02	0.21

https://doi.org/10.1017/CBO9780511761195.008 Published online by Cambridge University Press

6.6 Thick Triangular Element

The energy expressions for a thick plate element are given by expressions (6.64) to (6.67) of Section 6.3. The displacement functions

$$w = \sum_{j=1}^{3} L_j w_j, \qquad \theta_X = \sum_{j=1}^{3} L_j \theta_{X_j}, \qquad \theta_Y = \sum_{j=1}^{3} L_j \theta_{Y_j} \tag{6.190}$$

where $(w_j, \theta_{X_j}, \theta_{Y_j})$ are the degrees of freedom at node j and L_1, L_2, L_3 are area coordinates for the triangle, ensure that w, θ_X, θ_Y are continuous between elements. This element will be referred to as element THT.

Combining expressions (6.190) gives

$$\begin{bmatrix} w \\ \theta_X \\ \theta_Y \end{bmatrix} = [\mathbf{N}]\{\mathbf{w}\}_e \tag{6.191}$$

where

$$\{\mathbf{w}\}_e^{\mathrm{T}} = \lfloor w_1 \quad \theta_{X1} \quad \theta_{Y1} \quad w_2 \quad \theta_{X2} \quad \theta_{Y2} \quad w_3 \quad \theta_{X3} \quad \theta_{Y3} \rfloor \tag{6.192}$$

and

$$[\mathbf{N}] = \begin{bmatrix} L_1 & 0 & 0 & L_2 & 0 & 0 & L_3 & 0 & 0 \\ 0 & L_1 & 0 & 0 & L_2 & 0 & 0 & L_3 & 0 \\ 0 & 0 & L_1 & 0 & 0 & L_2 & 0 & 0 & L_3 \end{bmatrix} \tag{6.193}$$

Substituting (6.193) into the expression for the inertia matrix (6.74) and integrating using (4.90) gives

$$[\mathbf{m}]_e = [\mathbf{m}^{\mathrm{t}}] + [\mathbf{m}^{\mathrm{r}}] \tag{6.194}$$

where

$$[\mathbf{m}^{\mathrm{t}}] = \frac{\rho h A}{144} \begin{bmatrix} 24 & & & & & & & & \\ 0 & 0 & & & & & & & \\ 0 & 0 & 0 & & & & & \text{Sym} & \\ 12 & 0 & 0 & 24 & & & & & \\ 0 & 0 & 0 & 0 & 0 & & & & \\ 0 & 0 & 0 & 0 & 0 & 0 & & & \\ 12 & 0 & 0 & 12 & 0 & 0 & 24 & & \\ 0 & 0 & 0 & 0 & 0 & 0 & 0 & 0 & \\ 0 & 0 & 0 & 0 & 0 & 0 & 0 & 0 & 0 \end{bmatrix} \tag{6.195}$$

https://doi.org/10.1017/CBO9780511761195.008 Published online by Cambridge University Press

$$[\mathbf{m}^{\mathrm{r}}] = \frac{\rho h^3 A}{144}\begin{bmatrix} 0 & & & & & & & & \\ 0 & 2 & & & & & & & \\ 0 & 0 & 2 & & & & & \text{Sym} & \\ 0 & 0 & 0 & 0 & & & & & \\ 0 & 1 & 0 & 0 & 2 & & & & \\ 0 & 0 & 1 & 0 & 0 & 2 & & & \\ 0 & 0 & 0 & 0 & 0 & 0 & 0 & & \\ 0 & 1 & 0 & 0 & 1 & 0 & 0 & 2 & \\ 0 & 0 & 1 & 0 & 0 & 1 & 0 & 0 & 2 \end{bmatrix} \tag{6.196}$$

Substituting (6.191) into (6.66) and using (4.96) shows that the strain matrix due to flexure is

$$[\mathbf{B}^{\mathrm{f}}] = \frac{1}{2A}\begin{bmatrix} 0 & 0 & -a_1 & 0 & 0 & -a_2 & 0 & 0 & -a_3 \\ 0 & b_1 & 0 & 0 & b_2 & 0 & 0 & b_3 & 0 \\ 0 & a_1 & -b_1 & 0 & a_2 & -b_2 & 0 & a_3 & -b_3 \end{bmatrix} \tag{6.197}$$

As this is constant the integration of (6.80) is trivial. The stiffness matrix due to the flexure is therefore

$$[\mathbf{k}^{\mathrm{f}}] = \frac{h^3}{12} A[\mathbf{B}^{\mathrm{f}}]^{\mathrm{T}}[\mathbf{D}][\mathbf{B}^{\mathrm{f}}] \tag{6.198}$$

Substituting (6.191) into (6.66) and using (4.96) shows that the strain matrix due to shear is

$$[\mathbf{B}^{\mathrm{s}}] = \begin{bmatrix} \frac{a_1}{2A} & 0 & L_1 & \frac{a_2}{2A} & 0 & L_2 & \frac{a_3}{2A} & 0 & L_3 \\ \frac{b_1}{2A} & -L_1 & 0 & \frac{b_2}{2A} & -L_2 & 0 & \frac{b_3}{2A} & -L_3 & 0 \end{bmatrix} \tag{6.199}$$

Substituting (6.199) into (6.81) and integrating using (4.90) gives the following result for an isotropic material.

$$[\mathbf{k}^{\mathrm{s}}] = \kappa G h \begin{bmatrix} \mathbf{k}^{\mathrm{s}}_{11} & & \text{Sym} \\ \mathbf{k}^{\mathrm{s}}_{21} & \mathbf{k}^{\mathrm{s}}_{22} & \\ \mathbf{k}^{\mathrm{s}}_{31} & \mathbf{k}^{\mathrm{s}}_{32} & \mathbf{k}^{\mathrm{s}}_{33} \end{bmatrix} \tag{6.200}$$

where

$$\mathbf{k}^{\mathrm{s}}_{11} = \begin{bmatrix} \frac{(a_1^2 + b_1^2)}{4A} & -\frac{b_1}{6} & \frac{a_1}{6} \\ -\frac{b_1}{6} & \frac{A}{6} & 0 \\ \frac{a_1}{6} & 0 & \frac{A}{6} \end{bmatrix} \tag{6.201}$$

$$\mathbf{k}^{\mathrm{s}}_{21} = \begin{bmatrix} \frac{(a_2 a_1 + b_2 b_1)}{4A} & -\frac{b_2}{6} & \frac{a_2}{6} \\ -\frac{b_1}{6} & \frac{A}{12} & 0 \\ \frac{a_1}{6} & 0 & \frac{A}{12} \end{bmatrix} \tag{6.202}$$

https://doi.org/10.1017/CBO9780511761195.008 Published online by Cambridge University Press

$$\mathbf{k}_{31}^{s} = \begin{bmatrix} \dfrac{(a_3a_1 + b_3b_1)}{4A} & -\dfrac{b_3}{6} & \dfrac{a_3}{6} \\ -\dfrac{b_1}{6} & \dfrac{A}{12} & 0 \\ \dfrac{a_1}{6} & 0 & \dfrac{A}{12} \end{bmatrix} \tag{6.203}$$

$$\mathbf{k}_{22}^{s} = \begin{bmatrix} \dfrac{(a_2^2 + b_2^2)}{4A} & -\dfrac{b_2}{6} & \dfrac{a_2}{6} \\ -\dfrac{b_2}{6} & \dfrac{A}{6} & 0 \\ \dfrac{a_2}{6} & 0 & \dfrac{A}{6} \end{bmatrix} \tag{6.204}$$

$$\mathbf{k}_{32}^{s} = \begin{bmatrix} \dfrac{(a_3a_2 + b_3b_2)}{4A} & -\dfrac{b_3}{6} & \dfrac{a_3}{6} \\ -\dfrac{b_2}{6} & \dfrac{A}{12} & 0 \\ \dfrac{a_2}{6} & 0 & \dfrac{A}{12} \end{bmatrix} \tag{6.205}$$

$$\mathbf{k}_{33}^{s} = \begin{bmatrix} \dfrac{(a_3^2 + b_3^2)}{4A} & -\dfrac{b_3}{6} & \dfrac{a_3}{6} \\ -\dfrac{b_3}{6} & \dfrac{A}{6} & 0 \\ \dfrac{a_3}{6} & 0 & \dfrac{A}{6} \end{bmatrix} \tag{6.206}$$

The complete stiffness matrix for the element is

$$[\mathbf{k}]_e = [\mathbf{k}^{f}] + [\mathbf{k}^{s}] \tag{6.207}$$

The use of reduced integration for the shear stiffness matrix, as in the case of the thick rectangular element (Section 6.3), is not recommended [6.30].

Substituting (6.193) into (6.100) and assuming p_z to be constant gives the equivalent nodal force matrix

$$\{\mathbf{f}\}_e = \frac{p_z A}{3} \begin{bmatrix} 1 \\ 0 \\ 0 \\ 1 \\ 0 \\ 0 \\ 1 \\ 0 \\ 0 \end{bmatrix} \tag{6.208}$$

Therefore, one third of the total force is concentrated at each node.

Reference [6.31] presents a static solution for a simply supported square plate, of thickness to span ratio 0.1, which is subjected to a uniform load. It is demonstrated that the convergence is slow as the number of elements is increased. This

https://doi.org/10.1017/CBO9780511761195.008 Published online by Cambridge University Press

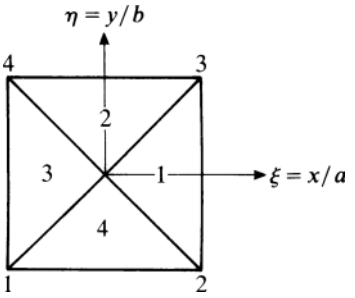

Figure 6.24. Geometry of a rectangular plate bending element.

reference also demonstrates that an improved rate of convergence can be obtained by representing the lateral displacement, w, by a quadratic function whilst still representing θ_X, θ_Y by linear functions. This rapid rate of convergence is also obtained when calculating the first two doubly symmetric frequencies of this same plate.

6.7 Other Plate Bending Elements

A conforming rectangular element has been developed in reference [6.32] using the smooth surface interpolation functions of reference [6.33]. Using the non-dimensional coordinates (ξ, η) defined in Figure 6.24, the displacement function is expressed in the form

$$w = \sum_{j=1}^{12} F_j(\xi, \eta)\alpha_j \tag{6.209}$$

The functions $F_j(\xi, \eta)$ are defined as follows

$$\begin{aligned} &F_1 = 1, \qquad F_2 = \xi^2, \qquad F_3 = \eta^2, \\ &F_4 = \xi, \qquad F_5 = \xi^3, \\ &F_7 = \eta, \qquad F_8 = \eta^3, \\ &F_{10} = \xi\eta, \quad F_{11} = 3\xi^3\eta + 3\xi\eta^3 - \xi^3\eta^3 - 5\xi\eta \end{aligned} \tag{6.210}$$

The remaining functions are defined by dividing the rectangle into four triangles by inserting the diagonals as shown in Figure 6.24.

$$F_6 = \begin{cases} \xi^2 - 2\xi + \eta^2 & \text{in region 1} \\ 2\xi\eta - 2\xi & \text{in region 2} \\ -\xi^2 - 2\xi - \eta^2 & \text{in region 3} \\ -2\xi\eta - 2\xi & \text{in region 4} \end{cases} \tag{6.211}$$

$$F_9 = \begin{cases} 2\xi\eta - 2\eta & \text{in region 1} \\ \eta^2 - 2\eta + \xi^2 & \text{in region 2} \\ -2\xi\eta - 2\eta & \text{in region 3} \\ -\eta^2 - 2\eta - \xi^2 & \text{in region 4} \end{cases} \tag{6.212}$$

$$F_{12} = \begin{cases} \frac{1}{4}(\xi^3\eta^3 - \xi^5\eta - 3\xi\eta^3 + 3\xi^3\eta) & \text{in regions 1, 3} \\ \frac{1}{4}(\xi\eta^5 - \xi^3\eta^3 - 3\xi\eta^3 + 3\xi^3\eta) & \text{in regions 2, 4} \end{cases} \tag{6.213}$$

https://doi.org/10.1017/CBO9780511761195.008 Published online by Cambridge University Press

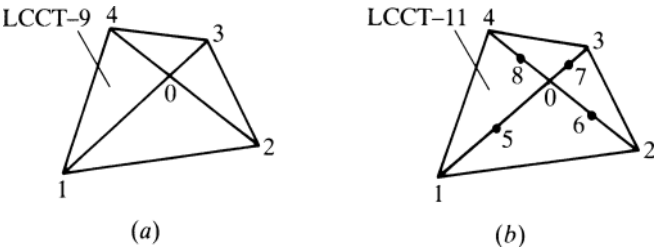

Figure 6.25. Geometry of element Q19: (*a*) inertia, (*b*) stiffness.

Functions F_1, F_4 and F_7 correspond to rigid body translation and rotation whilst F_2, F_3 and F_{10} correspond to constant curvature and twist. Also, functions F_7, F_8 and F_9 are the same as functions F_4, F_5 and F_6 rotated through 90° about the z-axis.

The coefficients α_j in (6.209) are expressed in terms of w, θ_x and θ_y at the four node points by the usual technique. The functions (6.210) to (6.213) define a cubic variation of w and a linear variation of the normal slope along the edges of the element. Therefore, the element is a conforming one. It will be referred to as the DP element.

Reference [6.28] presents a conforming quadrilateral (Q19) which has a linear variation of normal slope along each edge. The inertia matrix is obtained by assembling four LCCT-9 elements (Section 6.5.2). The element has, therefore, fifteen degrees of freedom (three at nodes 1, 2, 3, 4, 0 in Figure 6.25(*a*)). The stiffness matrix is obtained by assembling four LCCT-11 elements. An LCCT-11 element is derived from an LCCT-12 element (Section 6.5.2) by constraining the normal slope to vary linearly along one side. Therefore, the stiffness matrix has nineteen degrees of freedom, three at nodes 1, 2, 3, 4, 0 and one at nodes 5, 6, 7 and 8 in Figure 6.25(*b*). The degrees of freedom at nodes 5 to 8 are removed by static condensation (Section 4.6) leaving the matrix with fifteen degrees of freedom which is the same as the inertia matrix.

Reference [6.34] presents a conforming quadrilateral (CQ) with a quadratic variation of normal slope along each edge. The degrees of freedom are w, θ_x, θ_y at nodes 1, 2, 3, 4 and a normal slope at nodes 5, 6, 7, 8 (Figure 6.26). The element has, therefore, sixteen degrees of freedom. It is derived by dividing the quadrilateral into four sub-triangles and a cubic displacement function defined within each triangle. Reference [6.34] uses oblique axes for each triangle. The element has been rederived in reference [6.35] using area coordinates which are more convenient.

The displacement functions for each sub-triangle are expressed in terms of the seven degrees of freedom at the three external nodes and w, θ_x, θ_y at the internal

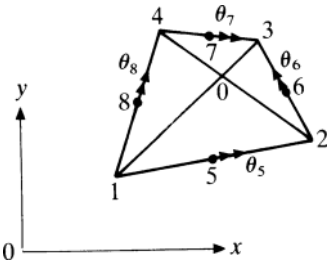

Figure 6.26. Geometry of element CQ.

https://doi.org/10.1017/CBO9780511761195.008 Published online by Cambridge University Press

Table 6.10. *Percentage difference between finite element and analytical frequencies of a simply supported square plate*

FEM grids ($\frac{1}{4}$ plate)	2×2		4×4	
Mode	(1, 1)	(1, 3)	(1, 1)	(1, 3)
DP	2.6	4.2	0.61	0.72
Q19	1.5	3.9	0.35	0.78
CQ	0.03	1.3	0.00	0.10

node 0. After assembling the four sub-triangles the three degrees of freedom at 0 are eliminated using continuity of normal slope between three pairs of sub-triangles.

The frequencies of the first two doubly symmetric modes of a simply supported square plate have been calculated using the above three elements. These frequencies are compared with the analytical frequencies in Table 6.10. Element Q19, which has three degrees of freedom more than element DP, produces only slightly better results. However, element CQ which has four degrees of freedom more than DP, gives much better accuracy.

Reference [6.36] presents a thick eight-node isoparametric element (RH) as shown in Figure 6.27. The displacements and geometry are represented by

$$w = \sum_{j=1}^{8} N_j w_j, \qquad \theta_x = \sum_{j=1}^{8} N_j \theta_{xj}, \qquad \theta_y = \sum_{j=1}^{8} N_j \theta_{y_j} \tag{6.214}$$

and

$$x = \sum_{j=1}^{8} N_j x_j, \qquad y = \sum_{j=1}^{8} N_j y_j \tag{6.215}$$

where the functions are identical to the ones defined for an eight-node membrane, that is (4.108) to (4.110). The inertia and stiffness matrices are evaluated using (3×3) and (2×2) arrays of integration points.

A simply supported square plate with a span/thickness ratio of 10 and $\nu = 0.3$ has been analysed using a (4×4) mesh of elements. The results obtained are compared with analytical values in Table 6.11. These show that greater accuracy is obtained than with an (8×8) mesh of four node elements (Table 6.5).

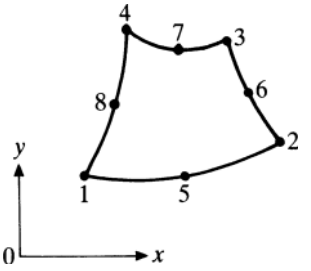

Figure 6.27. Geometry of an isoparametric element.

https://doi.org/10.1017/CBO9780511761195.008 Published online by Cambridge University Press

Table 6.11. *Comparison of predicted non-dimensional frequencies of a simply supported square plate. Element RH*

	$\lambda^{1/2}$		
Mode	FEM [6.36]	Analytical [6.21]	% Difference
(1, 1)	0.0931	0.0930	0.11
(2, 1)	0.2237	0.2218	0.86
(2, 2)	0.3384	0.3402	−0.53
(3, 1)	0.4312	0.4144	4.1
(3, 2)	0.5379	0.5197	3.5
(3, 3)	0.7661	0.6821	12.2

$\lambda = \rho h^2 \omega^2 / G$.

The main difference between thick and thin plates is that with thin plates the transverse shear strains γ_{xz}, γ_{yz} are negligible whilst for thick plates they are not. In developing a finite element model for thick plates it has been shown that continuity of w, θ_x, θ_y can easily be obtained by assuming independent functions for each. In the case of thin plates the vanishing of the transverse shear strains means that $\theta_x = \partial w/\partial y$ and $\theta_y = -\partial w/\partial x$. Thus w, θ_x, θ_y cannot be treated as independent and only a single function assumed for w. This leads to difficulties in ensuring that the normal slope is continuous between elements.

Another approach to developing a finite element for thin plates is the discrete Kirchhoff shear approach. This technique starts by assuming independent functions for w, θ_x, θ_y and then applies constraints to ensure that the transverse shear strains are zero at a discrete set of points.

Reference [6.37] presents several quadrilateral elements based upon this approach. For one of them (DKQ2), it is assumed that initially it has eight nodes, as shown in Figure 6.28. The displacement functions for w, θ_x, θ_y are taken to be (6.214). The degrees of freedom w, θ_n at nodes 5, 6, 7, 8 are eliminated by applying the constraints $\gamma_{xz} = 0$, $\gamma_{yz} = 0$ at a (2×2) array of Gauss points within the element. The degree of freedom θ_s at 5, 6, 7 and 8 is then eliminated by applying the constraint that θ_s varies linearly along each edge. In deriving the stiffness matrix the shear strain energy is ignored.

The accuracy of the frequency of the first two doubly-symmetric modes of a simply supported square plate obtained with the DKQ2 element and a consistent inertia matrix is indicated in Table 6.12. The meshes used for a quarter plate are (2×2) and (4×4). Reference [6.37] comments that the element is good for rectangular and parallelogram shapes but is not recommended for use as a general quadrilateral.

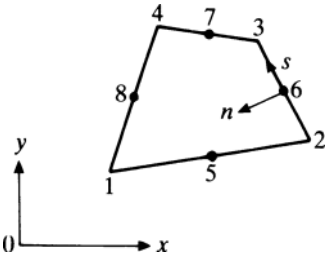

Figure 6.28. Geometry of the DKQ2 element.

https://doi.org/10.1017/CBO9780511761195.008 Published online by Cambridge University Press

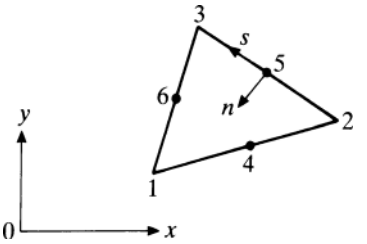

Figure 6.29. Geometry of the DKT element.

Reference [6.30] presents a triangular discrete Kirchhoff shear element (DKT). Initially, it is assumed that it has six nodes, as shown in Figure 6.29. The rotations θ_x, θ_y are assumed to vary quadratically over the element; therefore

$$\theta_x = \sum_{j=1}^{6} N_j \theta_{x_j}, \qquad \theta_y = \sum_{j=1}^{6} N_j \theta_{y_j} \tag{6.216}$$

where the functions N_j are given by (4.112). The degree of freedom θ_n at nodes 4, 5 and 6 is eliminated by requiring $\gamma_{sz} = 0$ at these points. In addition, the lateral displacement, w, is assumed to vary cubically along each edge. Thus for edge 2–3 (using (3.124))

$$\left(\frac{\partial w}{\partial s}\right)_6 = -\frac{3}{2l_{2-3}} w_2 - \frac{1}{4}\left(\frac{\partial w}{\partial s}\right)_2 + \frac{3}{2l_{2-3}} w_3 - \frac{1}{4}\left(\frac{\partial w}{\partial s}\right)_3 \tag{6.217}$$

The degree of freedom θ_s at nodes 4, 5 and 6 is eliminated by requiring this quantity to vary linearly along each side. Finally, the constraints $\gamma_{xz} = 0$ and $\gamma_{yz} = 0$ are applied at nodes 1, 2 and 3. The element is left with the degrees of freedom w, θ_x, θ_y at nodes 1, 2 and 3. The stiffness matrix is evaluated exactly using 3 integration points.

The results for a simply supported square plate using mesh sizes 2 and 4 (Figure 6.14) are given in Table 6.12. These results were obtained using a lumped diagonal mass matrix (more details of such representations are given in Chapter 12).

Reference [6.38] describes an improved discrete Kirchhoff triangular element which is referred to as the IMDKT element. Once again the rotations θ_x, θ_y are assumed to vary quadratically (6.212). θ_x, θ_y at nodes 4, 5, 6 (see Figure 6.29) are eliminated by assuming w to vary cubically and θ_s to vary linearly along each side. This gives

$$\begin{bmatrix} \bar{\theta}_x \\ \bar{\theta}_y \end{bmatrix} = \bar{\mathbf{N}}\mathbf{q} \tag{6.218}$$

Table 6.12. *Percentage difference between finite element and analytical frequencies of a simply supported square plate using discrete Kirchhoff shear elements*

Mesh size	2		3		4		5	
Mode	(1, 1)	(1, 3)	(1, 1)	(1, 3)	(1, 1)	(1, 3)	(1, 1)	(1, 3)
DKQ2	−1.1	+5.6			−0.3	−0.05		
DKT	−6.0	−16.0			−1.6	−3.2		
IMDKT	−0.45	+3.38	−0.3	+1.53			−0.15	+0.48

https://doi.org/10.1017/CBO9780511761195.008 Published online by Cambridge University Press

where

$$\mathbf{q}^{\mathrm{T}} = \lfloor w_1 \ \theta_{x1} \ \theta_{y1} \quad w_2 \ \theta_{x2} \ \theta_{y2} \quad w_3 \ \theta_{x3} \ \theta_{y3} \rfloor. \tag{6.219}$$

Assuming both θ_x, θ_y to vary linearly gives

$$\begin{bmatrix} \theta_x^* \\ \theta_y^* \end{bmatrix} = \mathbf{N}^* \mathbf{q} \tag{6.220}$$

It has been found that the best results are obtained using a combination of the two element displacement expressions (6.218) and (6.220), namely

$$\begin{bmatrix} \theta_x \\ \theta_y \end{bmatrix} = \hat{\mathbf{N}} \mathbf{q} \tag{6.221}$$

where

$$\hat{\mathbf{N}} = \bar{\mathbf{N}} + \lambda(\bar{\mathbf{N}} - \mathbf{N}^*) \tag{6.222}$$

and λ is a correction factor. The element stiffness matrix is now evaluated using (6.221) ignoring the shear strain energy. The inertia matrix is calculated using a combined displacement function

$$w = \bar{w} + \alpha(\bar{w} - w^*) \tag{6.223}$$

where $\bar{w}$ is assumed to vary cubically (see [6.39]) and w^* is a linear function. The results for a simply supported square plate using mesh sizes 2, 3, 4, 5 (Figure 6.14) and $\lambda = 0.08, \alpha = -0.1$ are given in Table 6.12.

Another technique of avoiding shear locking is to use mixed interpolation of the transverse displacements, rotations and transverse shear strains. A family of elements which use this approach is presented in reference [6.39]. These are referred to as MITC*n* elements, where *n* indicates the number of nodes.

The displacements of the rectangular MITC4 element, shown in Figure 6.30, are assumed to be of the form (6.68), namely

$$w = \sum_{j=1}^{4} N_j w_j, \qquad \theta_x = \sum_{j=1}^{4} N_j \theta_{xj}, \qquad \theta_y = \sum_{j=1}^{4} N_j \theta_{yj} \tag{6.224}$$

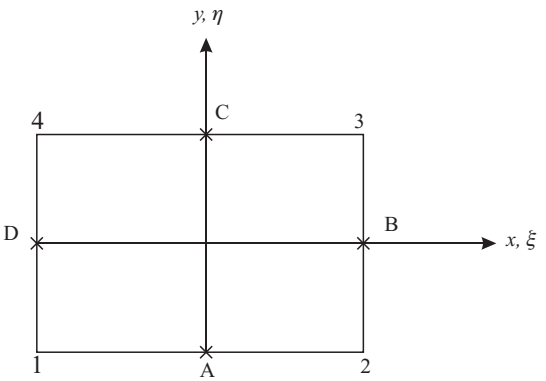

Figure 6.30. Geometry of the MITC4 element.

https://doi.org/10.1017/CBO9780511761195.008 Published online by Cambridge University Press

Table 6.13. *Percentage differences between MITC4 finite element and the results of reference [6.41] for a square plate of side L with mixed boundary conditions $h/L = 0.1$*

Mesh size whole plate	16	32	64
Mode			
1, 1	0.40	0.05	−0.005
2, 1	0.84	0.20	0.03
1, 2	1.76	0.44	0.10
2, 3	1.42	0.33	0.05

where the functions N_j are of bilinear form as given in equation (6.69). The shear strains are first calculated at the points A, B, C and D using equations (6.66) and (6.224). The shear strains at any other point within the element are then obtained from these by interpolation using

$$\begin{aligned} \gamma_{xz} &= \tfrac{1}{2}(1-\eta)\gamma_{xz}^{A} + \tfrac{1}{2}(1+\eta)\gamma_{xz}^{C} \\ \gamma_{yz} &= \tfrac{1}{2}(1-\xi)\gamma_{yz}^{D} + \tfrac{1}{2}(1+\xi)\gamma_{yz}^{B} \end{aligned} \tag{6.225}$$

The inertia and stiffness matrices are then formulated by substituting these expressions into (6.64) and (6.65) and using full Gaussian integration.

Reference [6.40] presents results for both a moderately thick plate ($h/L = 0.1$) and a thin plate ($h/L = 0.0001$) having simply supported, clamped, simply-supported, free boundaries. These are given in Tables 6.13 and 6.14. It can be seen that this element can be used for both moderately thick and thin plates.

In reference [6.43] the displacement function for a triangle is taken to be a complete quintic in x and y, a total of 21 terms. Three constraints are applied to ensure that the normal slope varies cubically over each edge of the triangle. The remaining 18 coefficients are expressed in terms of w, $\partial w/\partial x$, $\partial w/\partial y$, $\partial^2 w/\partial x^2$, $\partial^2 w/\partial x \partial y$ and $\partial^2 w/\partial y^2$ at the three vertices. The resulting element is a conforming one (NRCC).

The results for a simply supported square plate are compared with the analytical solution in Table 6.15. Although the results are extremely accurate, the predicted frequencies of the (1, 3) and (3, 1) modes are not equal as expected. Reference [6.44] presents an alternative formulation of this element and applies it to a number of polygonal plates.

Table 6.14. *Percentage differences between MITC4 finite element and the results of reference [6.42] for a square plate of side L with mixed boundary conditions $h/L = 0.0001$*

Mesh size whole plate	16	32	64
Mode			
1, 1	0.37	0.10	0.03
2, 1	0.79	0.23	0.09
1, 2	1.87	0.49	0.15
2, 2	1.51	0.40	0.13

https://doi.org/10.1017/CBO9780511761195.008 Published online by Cambridge University Press

Table 6.15. *Percentage difference between predicted and analytical frequencies for a simply supported square plate. NRCC element*

	Mesh size (Figure 6.14)		
Mode	1	2	3
(1, 1)	0.025	0.0005	0.0
(1, 2), (2, 1)	1.76	0.024	0.002
(2, 2)	2.44	0.036	0.003
(1, 3)	1.74	0.16	0.014
(3, 1)	2.09	0.26	0.023
(2, 3)	11.3	0.28	0.024

Table 6.16. *Percentage differences between predicted and analytical frequencies for a simply supported plate of aspect ratio 1.48:1. UM6 element*

	FEM grids ($\frac{1}{4}$ plate)		
Mode	1×1	2×2	3×3
1	0.014	0.0001	0.0
2	0.48	0.004	0.0005
3	0.61	0.002	0.0002
4	1.76	0.024	0.003
5	6.94	0.014	0.001

Table 6.17. *Natural frequencies (Hz) of a cantilever triangular plate of aspect ratio 1:1. Idealisation Figure 6.31(a)*

	Element			
Mode	DKT	LCCT-12	NRCC	Experimental [6.26]
1	34.5	36.6	36.6	34.5
2	117.6	140.7	139.3	136
3	155.6	196.0	194.0	190
4	271.1	344.0	333.4	325
5	331.2	475.8	454.2	441
6	403.7	629.7	590.5	578

$E = 206.7 \times 10^9$ N/m^2; $\nu = 0.3$; $\rho = 7890$ kg/m^3.

Table 6.18. *Natural frequencies (Hz) of a cantilever triangular plate of aspect ratio 1:1. Idealisation Figure 6.31(b)*

	Element		
Mode	LCCT-12/CQ	NRCC/UM6	Experimental [6.26]
1	36.6	36.5	34.5
2	139.7	139.0	136
3	194.7	193.6	190
4	339.7	332.6	325
5	463.3	452.9	441
6	607.6	588.7	578

E, ν, ρ as in Table 6.17.

https://doi.org/10.1017/CBO9780511761195.008 Published online by Cambridge University Press

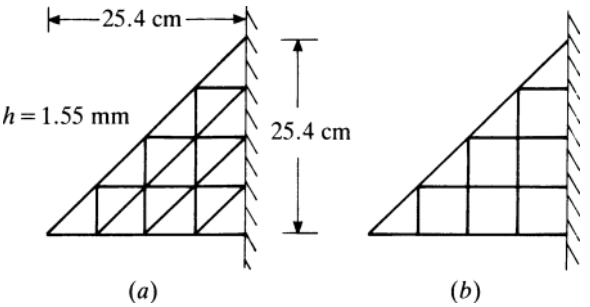

Figure 6.31. Idealisations of a cantilever triangle of aspect ratio 1:1.

Reference [6.45] presents a rectangular element, UM6, which is compatible with the NRCC element. It has the same degrees of freedom at the four corners and the same variation of displacement and normal slope over each edge. The results in Table 6.16 for a simply supported rectangular plate indicate its accuracy.

The natural frequencies of a cantilever triangle of aspect ratio 1:1 have been analysed using various triangular elements and the idealisation shown in Figure 6.31(a). The results are compared with measured frequencies in Table 6.17. The element DKT underestimates the frequencies whilst the other two overestimate them.

Figure 6.31(b) shows an idealisation which consists of a mixture of square and triangular elements. The frequencies predicted using two different pairs of compatible elements are compared with the measured ones in Table 6.18. These results show that they are more accurate than the corresponding ones in Table 6.17.

Problems

Note: Problems 6.2, 6.3, 6.5, 6.6 require the use of a digital computer.

6.1 Show that the stiffness matrix of the ACM element can also be expressed in the form $[\mathbf{C}]^{\mathrm{T}}[\mathbf{H}][\mathbf{C}]$ where $[\mathbf{C}] = [\mathbf{A}]_e^{-1}[\mathbf{d}]$. The matrix $[\mathbf{d}]$ is a diagonal matrix whose elements are 1, b, a repeated four times. Find $[\mathbf{H}]$ for the anisotropic case.

6.2 Use a (4×4) mesh of ACM elements to predict the six lowest frequencies of a square plate of side 1 m and thickness 2 mm which has all four edges fully clamped. Take $E = 207 \times 10^9$ N/m^2, $\nu = 0.3$, $\rho = 7850$ kg/m^3. Compare these frequencies with the analytical frequencies [6.46] 17.800, 36.304, 36.304, 53.528, 65.085, 65.391 Hz.

6.3 Figure P6.3(a) shows a square cantilever plate which has a stepped thickness as indicated. Use the idealisation of ACM elements shown in Figure P6.3(b) to calculate the nine lowest frequencies. Take $E = 206.84 \times 10^9$ N/m^2, $\nu = 0.3$ and

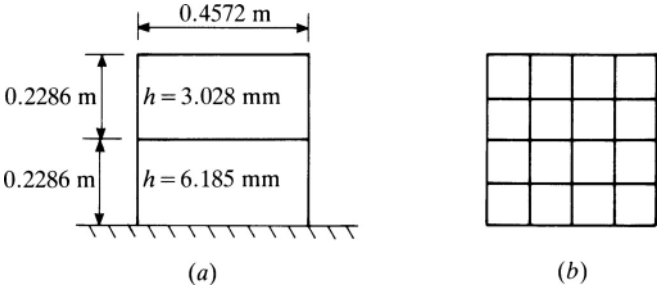

Figure P6.3. Geometry (a) and idealisation (b) of a stepped cantilever plate.

https://doi.org/10.1017/CBO9780511761195.008 Published online by Cambridge University Press

$\rho = 7853$ kg/m^3. Compare these frequencies with the experimental frequencies [6.47] 29.5, 56.6, 102.7, 129.8, 149.8, 264.4, 269.9, 308.5, 344.5 Hz.

6.4 If the thickness of the ACM element varies linearly, how many Gauss integration points are required to evaluate the inertia and stiffness matrices?

6.5 Figure P6.5(a) shows a rectangular cantilever with a wedge-shape cross-section. Use the idealisation of tapered ACM elements shown in Figure P6.5(b) to calculate the five lowest frequencies. Take $E = 206.84 \times 10^9$ N/m^2, $\nu = 0.3$, $\rho = 7861$ kg/m^3. Compare these frequencies with the experimental frequencies [6.48] 155.8, 668.4, 914.3, 1809.7, 2169.2 Hz.

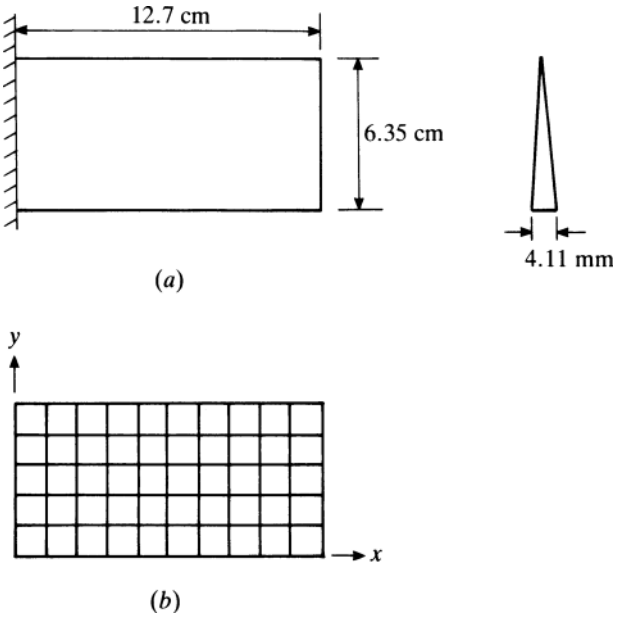

Figure P6.5. Geometry of a cantilever with a wedge shaped cross-section.

6.6 repeat Problem 6.5 using constant thickness ACM elements. Define the thickness of an element to be its average thickness.

6.7 Show that the displacement function defined by (6.17), (6.50) and (6.51) is a conforming one by evaluating w and θ_y on the side $\xi = 1$.

6.8 Show that the displacement function defined by (6.17), (6.52) and (6.53) gives continuity of w, θ_x, θ_y and w_{xy}.

6.9 Show that the displacement function defined by (6.17), (6.51), (6.61), (6.62) and (6.63) is a non-conforming one by evaluating w and θ_y on the side $\xi = 1$.

6.10 Show that the first six terms in (6.5) are present in the displacement function defined in Problem 6.9.

6.11 Show that the inertia matrix (6.75) gives the correct mass and moments of inertia.

6.12 Derive the stiffness matrix due to transverse shear strain energy for a rectangular thick plate bending element using equations (6.66), (6.224) and (6.225).

https://doi.org/10.1017/CBO9780511761195.008 Published online by Cambridge University Press

6.13 Derive expressions for the inertia, stiffness and equivalent nodal force matrices for a quadrilateral version of the HTK thick plate element, presented in Section 6.3.

6.14 Show that the inertia matrix (6.194) gives the correct mass and moment of inertia about an axis through nodes 1 and 2.

6.15 The displacement functions for a thick triangular element are assumed to be

$$w = \alpha_1 + \alpha_2 x + \alpha_3 y + \alpha_4 x^2 + \alpha_5 xy + \alpha_6 y^2$$

$$\theta_x = \beta_1 + \beta_2 x + \beta_3 y$$

$$\theta_y = \gamma_1 + \gamma_2 x + \gamma_3 y$$

Show that the assumption that Q_s is constant along each side, where s is along a side, leads to the relationships

$$\alpha_4 = -\tfrac{1}{2}\gamma_5 \qquad \alpha_5 = \tfrac{1}{2}(\beta_2 - \gamma_3), \qquad \alpha_6 = \tfrac{1}{2}\beta_3$$

https://doi.org/10.1017/CBO9780511761195.008 Published online by Cambridge University Press